Naval Research Laboratory
Washington, DC 20375-5320

NRL/MR/6180--00-8446

Modeling Missile Propellant Fires In Shipboard Compartments

PATRICIA A. TATEM
FREDERICK W. WILLIAMS

Navy Technology Center for Safety and Survivability
Chemistry Division

DEREK A. WHITE
CRAIG L. BEYLER

Hughes Associates, Inc.
Baltimore, MD

March 30, 2000

REPORT DOCUMENTATION PAGE

Form Approved
OMB No. 0704-0188

1. AGENCY USE ONLY (*Leave Blank*)	2. REPORT DATE	3. REPORT TYPE AND DATES COVERED
	March 30, 2000	October 1998 — September 1999

4. TITLE AND SUBTITLE

Modeling Missile Propellant Fires In Shipboard Compartments

5. FUNDING NUMBERS

PE – 63508N

6. AUTHOR(S)

P.A. Tatem, F.W. Williams, D.A. White,* and C.L. Beyler*

7. PERFORMING ORGANIZATION NAME(S) AND ADDRESS(ES)

Naval Research Laboratory
Washington, DC 20375-5320

8. PERFORMING ORGANIZATION REPORT NUMBER

NRL/MR/6180--00-8446

9. SPONSORING/MONITORING AGENCY NAME(S) AND ADDRESS(ES)

Office of Naval Research
800 N. Quincy Street
Arlington, VA 22217

10. SPONSORING/MONITORING AGENCY REPORT NUMBER

11. SUPPLEMENTARY NOTES

*Hughes Associates, Inc., Baltimore, MD

12a. DISTRIBUTION/AVAILABILITY STATEMENT

Approved for public release; distribution unlimited.

12b. DISTRIBUTION CODE

13. ABSTRACT (*Maximum 200 words*)

Concerns regarding the likelihood and severity of missile propellant fires resulted in a test program to characterize this class of fire. Full-scale test programs have investigated the phenomena associated with propellant fires. An existing computer fire model, FAST, was modified to account for fire phenomena specific to missile propellant combustion. The modified computer program and the developed missile propellant burning rate algorithm were exercised in blind predictions of full-scale tests. The model predictions characterize the compartment environment (e.g. gas temperatures, layer interface, oxygen concentration, visibility and heat flux on floor targets) which is important in ascertaining the likelihood of subsequent ignition of class A materials in the compartment. Comparisons between the blind predictions and the test data are presented. These components show a good level of agreement between the test data and modeling predictions.

14. SUBJECT TERMS

Missile propellant
Fire modeling
Shipboard compartments
Full-scale tests
Class A materials
Ignition

15. NUMBER OF PAGES

52

16. PRICE CODE

17. SECURITY CLASSIFICATION OF REPORT	18. SECURITY CLASSIFICATION OF THIS PAGE	19. SECURITY CLASSIFICATION OF ABSTRACT	20. LIMITATION OF ABSTRACT
UNCLASSIFIED	UNCLASSIFIED	UNCLASSIFIED	UL

NSN 7540-01-280-5500

Standard Form 298 (Rev. 2-89)
Prescribed by ANSI Std 239-18
298-102

CONTENTS

MODELING MISSILE PROPELLANT FIRES IN SHIPBOARD COMPARTMENTS

1.0 INTRODUCTION

Concerns regarding the likelihood and severity of propellant initiated fires have given rise to a test program to characterize this class of fires [1-4]. This test program was very successful in identifying the basic character of these fires and the important phenomenology which govern the ultimate results. Several phenomena unique to propellant-initiated fires have been identified, including overpressures which result from the propellant burn and the dependence of Class A material ignition upon the interplay of temperature and oxygen concentration at the end of the propellant burn.

Missile propellant fires result in interesting phenomena which have been observed during the experiments. The fire growth rate associated with the ignition of the missile propellant results in a jump to tens of megawatts in a matter of seconds. A measurable overpressure surge pushes the compartment air, with normal oxygen content, out as it is filled with expanding combustion gases from the burning missile propellant. As the missile propellant continues to burn, the compartment is assaulted with high radiant heat fluxes and gas temperatures which can globally exceed peak values of 1200 to 1400°C. This severe thermal exposure only lasts for approximately a minute which corresponds to the propellant burning duration. The heating of the compartment and its contents occurs in the brief window of time where the oxygen content of the compartment environment is significantly depressed. As fresh air with normal oxygen content begins to re-enter the compartment, the combustible items which were only briefly heated, have begun to cool. Thus, an interplay of the surface temperatures of combustible items and the local oxygen concentrations determines the possibility of ignition.

As is often the case, it is not feasible to test all combinations of parameters which may be expected in practice, and it can be difficult to extrapolate the results from this test series to the broad range of ship compartments and burn scenarios of interest within the U.S. Navy Fleet. In order to consolidate the findings from the experimental program and facilitate the application of the results to a broad range of ship compartments and scenarios, a model capable of simulating the impact of these fires was developed.

The focus of this project was an evaluation of the feasibility of modeling propellant-initiated fires by attempting to predict the results of the HULVUL tests [3] without prior examination of the experimental results. The test results of the China Lake series [1,2] were used to guide model development. The goal of the work has been to develop a tool with sufficient capabilities to

Manuscript approved February 29, 2000.

characterize the fire environment in the compartment with burning missile propellant. No attempt has been made to predict conditions in compartments other than the compartment of fire origin.

2.0 MODEL SELECTION

In the interest of efficiency, it was desirable to build on an existing model, rather than develop a specialized model. A review of the experimental results and the goals of the program showed that these fires could be modeled using the zone approach widely used in compartment fire modeling. The zone modeling approach assumes that the compartment environment can be described as two uniform layers, a hot layer and a cold layer. A number of candidate zone type fire models are available which may be modifiable to predict propellant initiated fires onboard ships [5- 9].

FAST was chosen for this work based on its treatment of pressure and its ability to model fire sources which do not require oxygen in the compartment to support combustion. The FAST formulation solves a time-dependent ordinary differential equation (ODE) for pressure. Other models that were considered use the quasi-steady assumption for pressure. Trial runs showed that the rapidly increasing heat release rates associated with missile propellant fires caused numerical problems for computer models using the quasi-steady approach. Further, FAST includes an option for an unconstrained fire which allows the simulation of a prescribed heat release rate history regardless of the available oxygen in the compartment. Since propellants include their own oxidizer, this is an appropriate model for missile propellant fires.

The use of the unconstrained option in FAST for ordinary combustibles is not appropriate. The inclusion of unconstrained fires in FAST is a historical vestige of the model's development and not a feature which ordinarily has any useful purpose. For those who have come to CFAST modeling in recent years, it is important to note that the FAST name has been recycled by NIST to refer to the CFAST interface as FAST. Where the notation FAST is used in this paper, it refers to the fire model predecessor to CFAST and not to the more recent interface to CFAST.

3.0 MODEL MODIFICATIONS

The source code for FAST, Version 18.5.3.2, was obtained from NIST for use in this effort. FAST, Version 18.5.3.2, was the most advanced version of the program available at the time of the project. After this work was completed, FAST was eventually superceded by CFAST. For the purposes of this project, it was judged that only the convective and radiative heat transfer algorithms used by FAST needed to be modified. The convection heat transfer model found in FAST uses correlations based on natural convective flow. In actuality, the fire compartment wall heat transfer is dominated by forced convection processes. Typically, forced convection heat transfer coefficients are significantly larger than natural convection. The algorithm used to model wall convection heat transfer in this project was the algorithm developed for and implemented in the Harvard Fire Code [9]. The heat transfer coefficient is 5 kW/m^2 at ambient temperature and increases linearly to 50

kW/m^2 at 100 C above ambient and remains at that level at higher gas temperatures. This yields convective heat transfer coefficients that are roughly an order of magnitude greater than those found in the basic FAST algorithm. This method was used on the fire side of the compartment bulkheads, and the unmodified FAST method was used on the unexposed bulkhead surfaces.

The FAST radiation heat transfer model, which calculates the radiant exchange from the hot layer to the bounding surfaces, assumes that the emissivity of the hot layer is universally 0.5. In the absence of any smoke concentration data, this is a defensible estimate for the preflashover stage of the fire. However, the very high concentration of aluminum oxide particles in the layer assures that the layer is optically thick. Ideally, one would calculate the layer emissivity from the particle concentration using widely known methods [10]. However, since the unconstrained fire option does not calculate species concentrations, this is not possible. For this project, the algorithm was simply altered to use a constant emissivity of 1.0. Given the high particle concentrations found in the experiments, this should give excellent agreement with the tests for the period where the rocket propellant combustion dominates the compartment environment.

The current version of CFAST uses an absorption coefficient of 0.5 1/m for unconstrained fires. For all but the smallest compartments, this means that the current CFAST model assumes that hot layers are effectively black for unconstrained fires, as was done with the modified FAST in this work. The current CFAST model continues to use the old natural convection correlations so that the modified FAST convection algorithm used in this work remains a departure from the current CFAST convection algorithm. Of course, other changes to CFAST have been made during the 1990's, including major revisions to other aspects of radiative exchange. Limited simulations have been made with the current version of CFAST and the results are very similar to the results presented in this paper if a radiative fraction of about 0.3 is used. If no radiation from the fire source is included in the current CFAST as was done in FAST, the layer temperatures tend to be somewhat high (~150C). It is significant that in this work, compartment pressures were well predicted, but with the current CFAST the pressures are very significantly underpredicted. The reasons for this serious and systematic underprediction are unclear. Because the differences in the pressure predictions from FAST and CFAST could not be understood or rationalized, pressure results are not presented in this paper.

4.0 DEVELOPMENT OF THE MISSILE PROPELLANT BURNING RATE RELATIONSHIP

Simulating the burning of missile propellant requires the identification of both the burning rate (mass loss) history and the heat of combustion of the propellant. The burning rate history must be expressed in kilograms per second as a function of time over the burning duration. The heat of combustion of the HV-1 propellant used in the China Lake and HULVUL test is known to be 8.4 MJ/kg [1]. Ascertaining the mass loss rate history through experimental means is extremely difficult due to the large forces generated by the burning propellant. In the absence of empirical data to define

the mass loss rate history, a reasonable estimate can be made based on the physical characteristics of the fuel package (i.e., total mass, shape, and dimensions) and a simple combustion model.

Although the prediction of missile propellant burning is very complex process, reasonable estimates can be made using relatively simple methods. Two burning regimes can be identified. The initial growth period is defined from ignition to the peak burning rate which is driven by the rate at which combustion spreads from the ignition area to encompass the entire exposed surface area of the propellant. This initial growth period is relatively short in comparison to the overall burning duration. The decay period is defined from the peak burning rate to the complete consumption of the fuel package at the end of the burn. The burning rate in this regime is determined by the linear regression rate of the specific missile propellant and the resulting change in surface area. The decay burning regime represents the largest portion of the total burning duration.

No firm theoretical basis for predicting the flame spread process over the exterior, exposed surface of the propellant fuel package was identified. Careful examination of the China Lake test data confirmed that this process requires only a few seconds. The radiometers which faced the propellant provided the data which showed that the rise time to the peak irradiance was on the order of 4 to 16 seconds with a six second average over all tests.

The rise time to peak irradiance was equated with the time to peak burning rate which defines the initial growth period. The burning rate was assumed to increase linearly during the initial growth period. The simulations of the China Lake test series used the test specific rise time from the radiometer data. The blind HULVUL test simulations used the 6 second average rise time from the China Lake series.

The China Lake simulations also used a linear decay in mass loss rate based on a total burning duration of 60 seconds, estimated from visual observations. The blind HULVUL simulations used the following model for the decay regime. The decay regime burning is driven by the linear regression rate, V, which for most propellants can be expressed as:

$$V = CP^n \qquad (1)$$

where P is the pressure. For propellants like HV-1, at atmosphere pressure, regression rates on the order of 2 mm/s are reported and values of n are about ½ [11].

The majority of the China Lake and HULVUL tests used cylindrical missile propellant fuel elements. While the reported regression rates are linear regression rates [11], it is possible to apply them to other geometrically shaped fuel packages. Specifically, this approximation should be accurate until the radius becomes small, which fortunately is close to the end of the burn when the total mass burning rate is small.

Incorporating the linear regression rate into the expression for the mass burning rate yields

$$\dot{m} = V\rho A \tag{2}$$

where ρ is the propellant density and A is the exposed surface area and V is the regression rate.

The mass burning rate is dependent upon the surface area of the cylindrical fuel element, which experiences a decreasing effective radius and cylinder length as a result of burning over both ends and the cylindrical surfaces of the cylinder. For a cylindrical fuel element the surface area is given by

$$A = 2\pi RL + 2\pi R^2 \tag{3}$$

where R (m) and L (m) are the time varying quantities:

$$\begin{aligned} R &= R_o - Vt \\ L &= L_o - 2Vt \end{aligned} \tag{4}$$

Substituting Equation 3 into Equation 2 yields:

$$\dot{m} = V\rho\,[2\pi\,(R+L)\,R] \tag{5}$$

The burning rate begins at its maximum value and decreases with time until the radius of the cylinder goes to zero. The duration of burning, t_b, is simply the time until the effective radius reaches zero.

$$t_b = \frac{R_o}{V} \tag{6}$$

The cylindrical fuel packages used in the China Lake and HULVUL tests had a radius of 0.127 m. Assuming that V=0.002 m/s, the burning duration is 63.5 seconds which closely approximates the burn time visually observed for these 0.127 m radius cylindrical fuel packages.

The burning duration for the more general cylinder case is the minimum of R_o/V and $0.5\ L_o/V$, assuming both ends are burning. In the more general cylinder solution with end effects included, the burning rate is given by

$$\dot{m} = V \rho \left[2\pi (R_0 - Vt)(L_o - Vt) + 2\pi (R_o - Vt)^2\right]$$

$$t_b = \min\left(\frac{R_o}{V}, \frac{L_o}{2V}\right) \tag{7}$$

Normalizing the burning rate by the initial burning rate, $\dot{m}_o$, and rearranging to eliminate V yields

$$\frac{\dot{m}}{\dot{m}_o} = \frac{\left(1 - \min\left(1, \frac{L_o}{2R_o}\right)\left(\frac{t}{t_b}\right)\right)\left(\frac{L_o}{R_o} + 1 - 3\min\left(1, \frac{L_o}{2R_o}\right)\left(\frac{t}{t_b}\right)\right)}{\frac{L_o}{R_o} + 1} \tag{8}$$

This equation indicates that the normalized mass loss rate is simply a function of the burning duration and the aspect ratio of the fuel cylinder. Figure 1 shows the normalized burning rate as a function of the normalized time, t/t_b, for a range of aspect ratios, L_o/R_o. The Figure clearly shows the two limiting cases; the constant burning rate (end dominated) case, and the linear burning rate (cylindrical surface dominated) case. Most of the fuel cylinders used in the China Lake and HULVUL test series had an aspect ratio ranging from 2 to 8 depending on the quantity of missile propellant used. In the China Lake comparisons, the model input used was the linear case which ignores end effects. In the HULVUL test predictions, the generalized relationship of Equation 7 was used to describe the burning rate. As Figure 1 indicates, the differences between these cases are not great.

Other fuel element geometries can be handled using these same methods. If the linear burning velocity is known for the propellant and the fuel element can be characterized in terms of a simple geometric shape, the burning rate history required for modeling can be determined.

5.0 CHINA LAKE TEST DESCRIPTIONS

The China Lake test series used a steel mock-up of shipboard compartments. The test data collected in the initial China Lake test series were used to direct the model development.

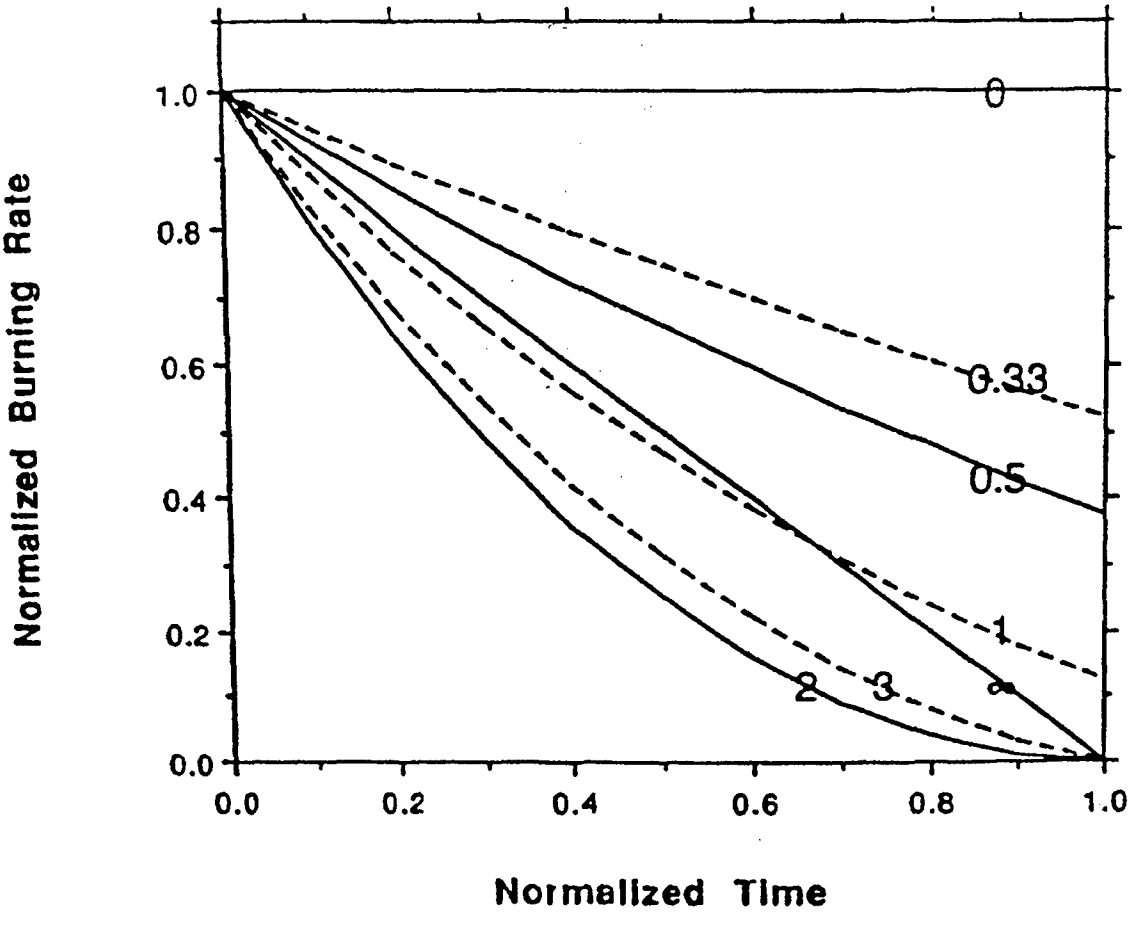

Figure 1 – Burning rate of a cylindrical fuel element as a function of time and aspect ratio L_o/R_o

The model was then exercised to blindly predict the experiments performed in the HULVUL test series. The compartment testing configuration, ventilation arrangements, instrumentation and fuel configuration have been described for the China Lake tests series in References 1 and 2, and are summarized in the following section..

5.1 China Lake Simulated Shipboard Compartment Test Configuration

The shipboard compartment simulator consisted of three compartments: a vented burn compartment (6.1 x 6.1 x 3.1 m), an adjacent compartment (4.6 x 4.6 x 3.1 m), and an overhead compartment (4.6 x 4.6 x 3.1 m). An isometric view and a plan view of the ship compartment simulator are presented in Figures 2 and 3, respectively. Structurally, the compartments were constructed from steel with 0.95 cm thick steel plate used for bulkheads and 1.27 cm thick steel plate used for decks and overheads. The bulkheads were reinforced with 15.2 cm I-Beams on 1.5 m centers. The deck plating was reinforced underneath with 30.5 cm I-Beams on 1.5 m centers and the structural integrity of the burn compartment was augmented by the inclusion of several 15.2 cm I-Beams columns.

5.2 China Lake Test Series

The China Lake solid rocket propellant combustion tests were performed in order to characterize the thermal environments generated in simulated shipboard compartments. These tests were performed prior to the British Hull Vulnerability Trails jointly conducted by the U.S. Navy and the Royal Navy. The first seventeen scoping tests investigated the impact of various quantities of solid rocket propellant, 11.3 to 95.3 kilograms, over varying vent sizes. The final fourteen tests generally focused on a 68.0 kilogram missile propellant fuel load with varying vent sizes. The purpose was to establish a relationship between the fire compartment conditions as a function of the fuel load and ventilation area. Eleven tests were conducted with the full vertical vent height, 2.9 m, with various opening widths (0.15 to 1.22 m). Six additional tests were conducted utilizing various single and double vent configurations.

There were two adjacent 1.5 mm diameter Type K inconel-sheathed thermocouple trees in each compartment, consisting of 10 thermocouples with 0.31 m spacing beginning at 0.15 m above the deck. One of these thermocouple trees was air aspirated with a flow velocity of about 5 m/s. The aspiration had no measurable effect on the measured temperatures. Additionally, there was a Type K exposed bead (0.4 mm diameter) thermocouple tree located in the center of the vent, that utilized the same spacing as the compartment trees. Bulkhead thermocouples were peened into both sides of two bulkheads at the bulkhead centerline at a 0.6 m vertical spacing.

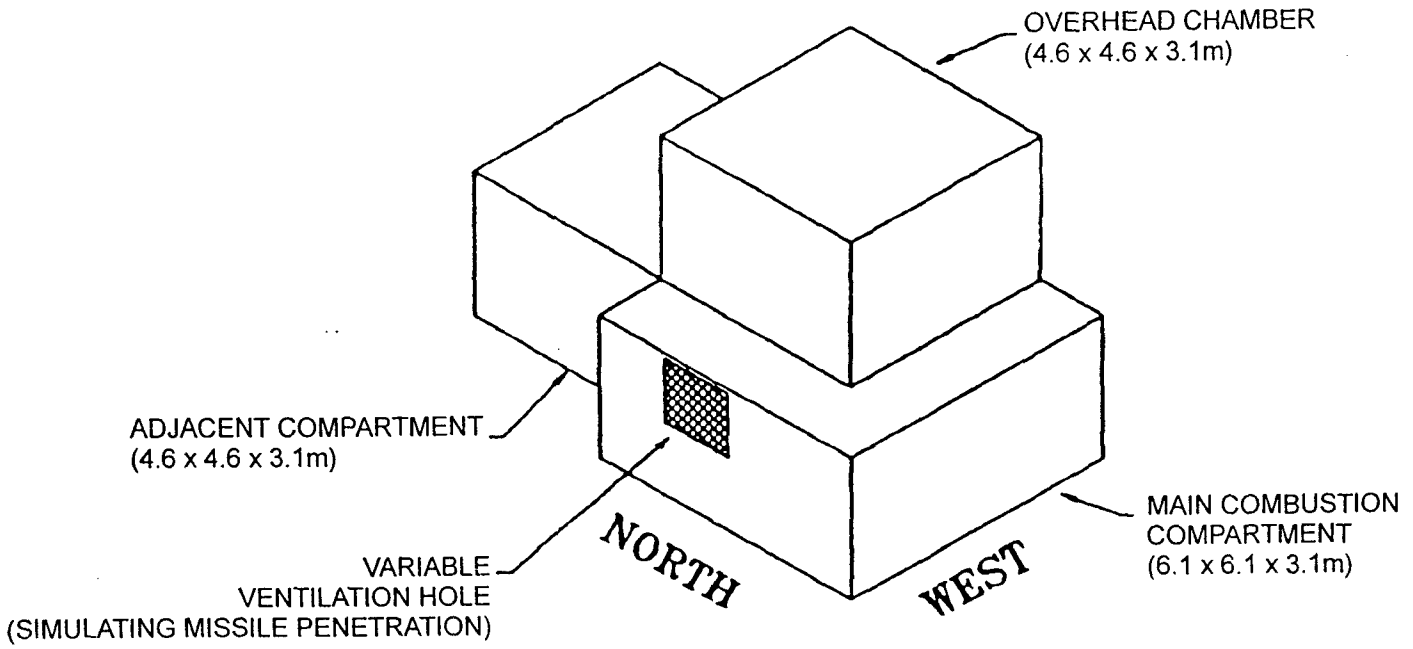

Figure 2 – Isometric view of ship compartment simulator

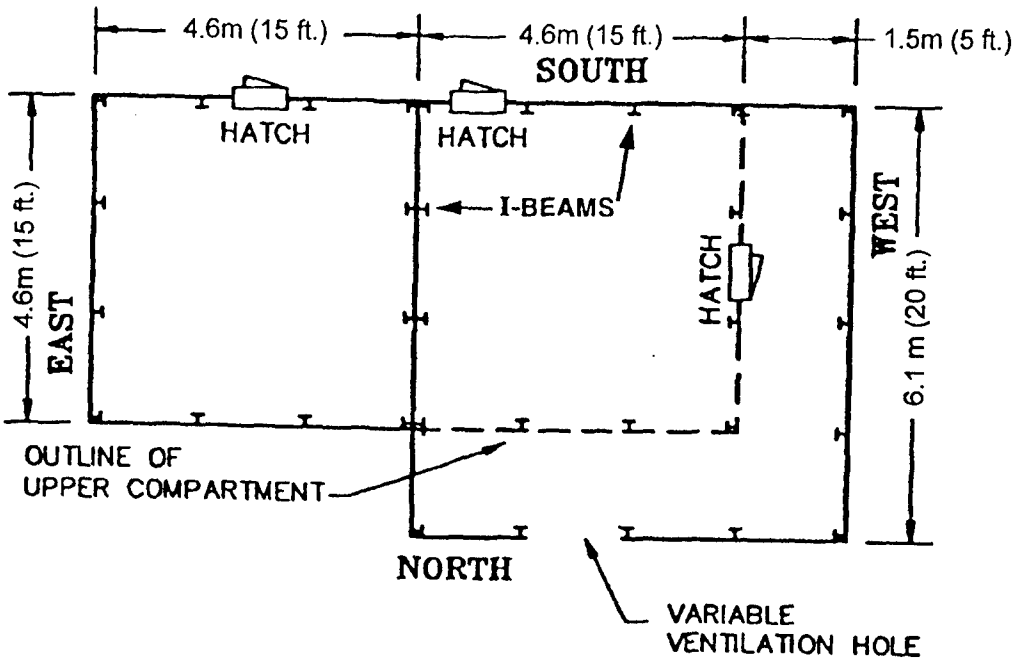

Figure 3 – Ship compartment simulator, plan view

Total heat flux transducers were installed in the center of the deck and overhead of the burn compartment. Four water cooled Schmidt-Boelter radiometers (range 0-250 kW/m^2) with 150 degree sapphire windows were installed in the main compartment: two facing the propellant burn table (fire brick on a steel table) at a distance of 1.5 m and 3.1 m, both at an elevation of 0.31 m; and one each in the deck and overhead of the northeast corner. Pressure transducers were installed on the north and south bulkheads of the main compartment at 0.31 m above the deck. Gas sampling points for O_2, CO_2, and CO were installed 0.31 m below the overhead and an additional O_2 sampling point was installed 0.31 m above the deck for the final fourteen tests (to help assess the potential for ignition of Class A materials). The instrumentation layout used for the China Lake test series is shown in Figure 4.

5.3 China Lake Test Results

This test series was used to identify important phenomena which needed to be modeled and to assist in the development of model modifications and methods for determining model inputs. As such, the predictions of the China Lake test series were performed with prior knowledge of the test results. For this reason, the goal of this section is simply to demonstrate that the model can be made to function sufficiently well to expect to be able to predict the HULVUL tests without prior knowledge of the results.

5.3.1 China Lake Test Series- Sample Comparisons Between the Modeling Results and Test Results

Comparisons for Test 20, which used 68.2 kg (150 lb) of HV-1 with a 0.3 m by 2.9 m vent, will be shown in detail to illustrate the general level of agreement. China Lake Test 20 demonstrates the typical level of agreement in the test series.

The comparison of upper layer temperatures for Test 20 is shown in Figure 5. The peak temperature is underpredicted by 150°C, and the predicted peak temperature time is several seconds after the measured peak. Overall, the temperature prediction is accurate to within 150°C over the period of the propellant burn. The measured temperature used for the comparison is the top thermocouple of the vent tree. Typically, the upper thermocouples in the vent give good indications of the upper layer in the compartment. Figure 6 shows temperatures measured at various locations in the upper half of the compartment. The difference in shape between the vent tree and the compartment tree may be attributed to the different response times associated with the bare bead thermocouples (quicker response) used in the vent tree and the inconel-sheathed thermocouples (slower response) used in the compartment tree. The figure indicates that the prediction is a reasonable representation of the conditions in the upper layer. A more quantitative assessment of the quality of the predictions is included in the next section.

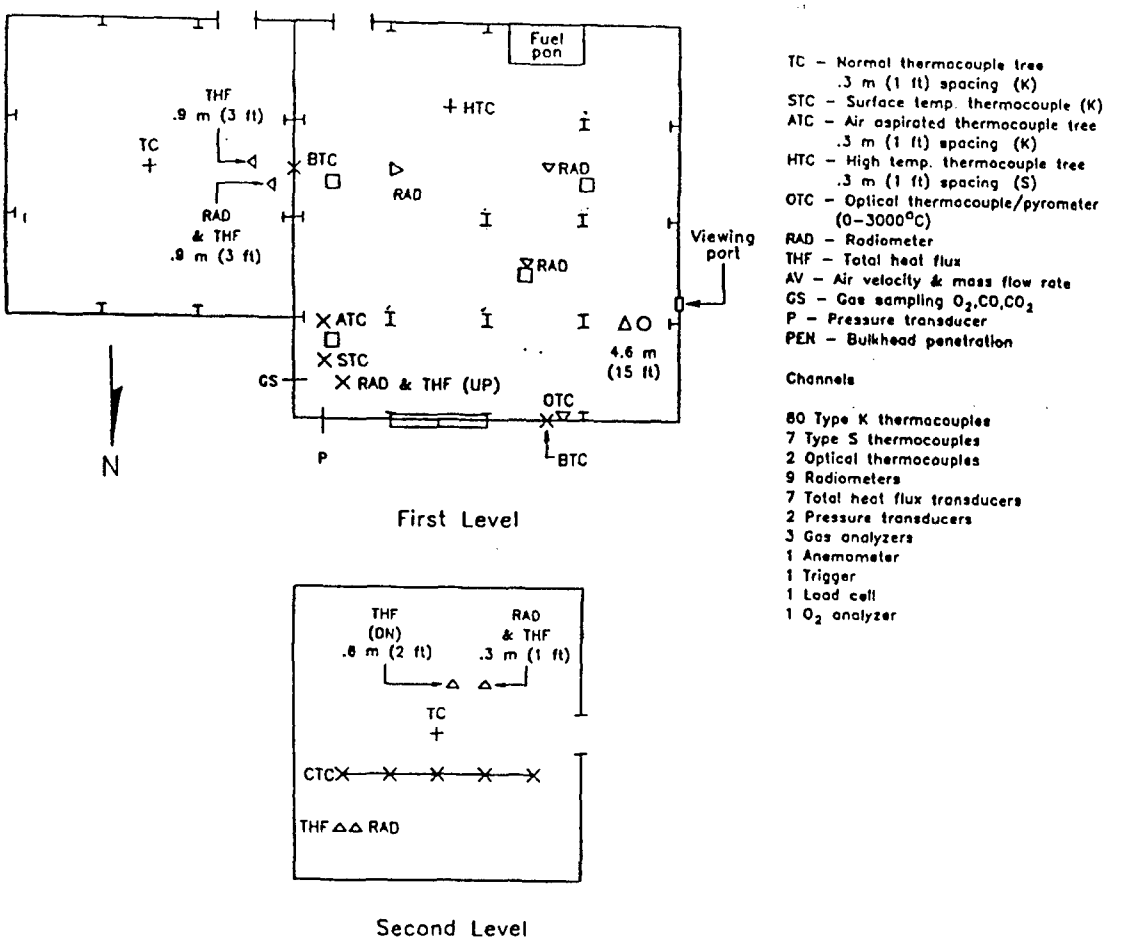

Figure 4 – China Lake test series instrumentation layout

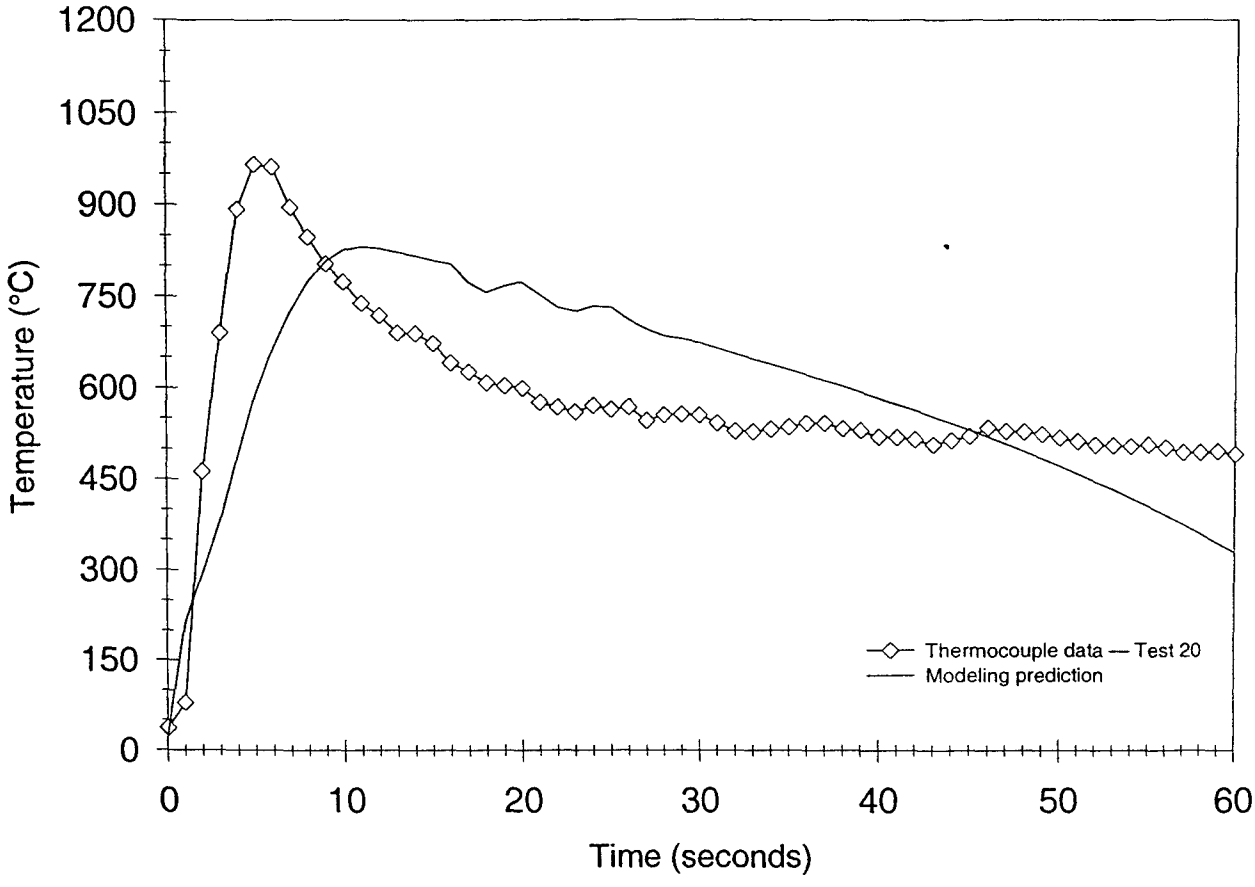

Figure 5 – Modeling prediction compared to Test 20 data, upper layer temperature

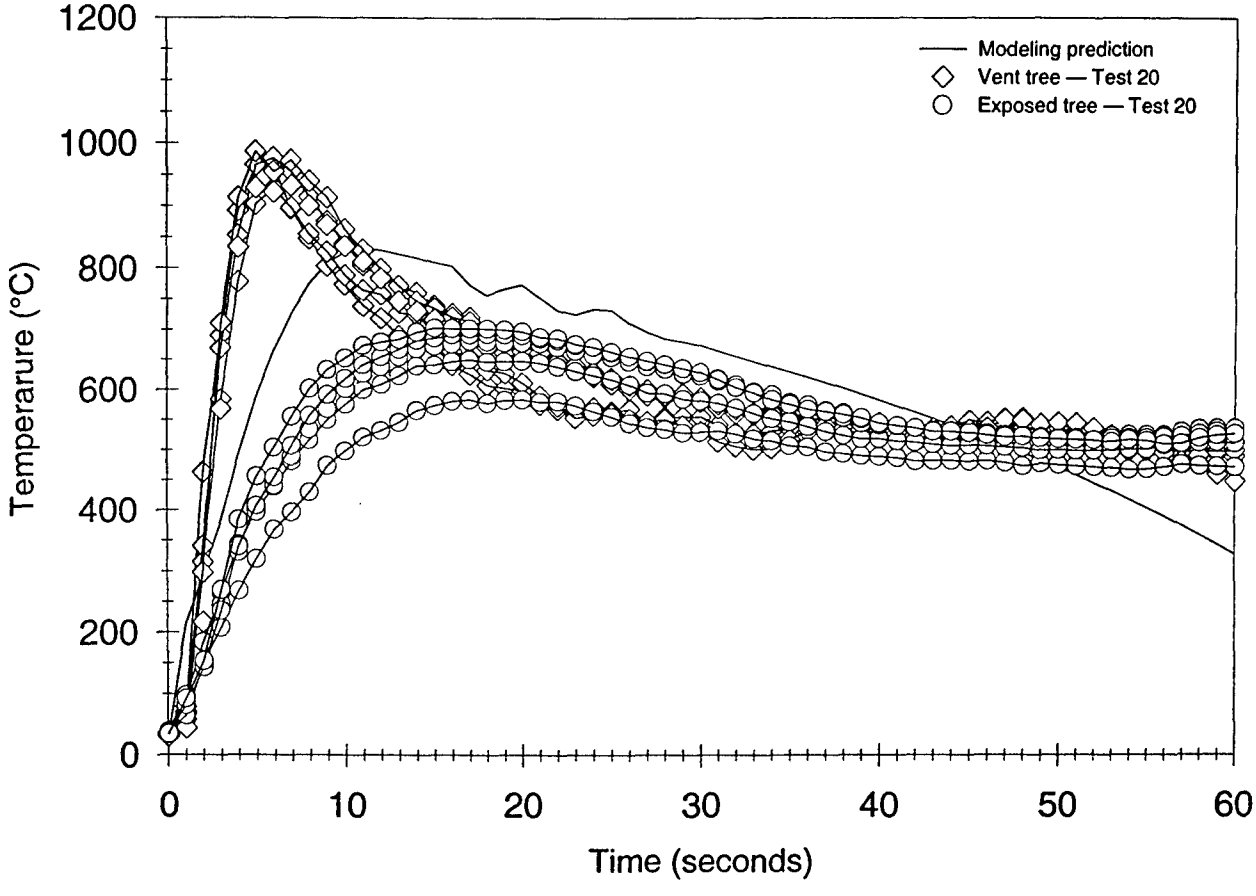

Figure 6 – Temperatures recorded in the upper half of the compartment China Lake, Test 20

In all tests, the heating of the bulkheads by the propellant burn was quite modest. Figure 7 shows a comparison of the predicted and measured bulkhead temperatures for Test 20. The agreement is generally good and is typical of the results found throughout the China Lake test series comparisons.

Figure 8 show a comparison of the predicted heat flux to the floor and the measured radiative heat flux to the floor. The comparison shows that the heat fluxes are greatly overpredicted by the model after 10 s into the run. This is not consistent with the layer temperature prediction, which is far better. The low measured heat fluxes are likely to have been the result of aluminum oxide buildup on the upward facing transducer surfaces.

These comparisons of experimental and model results show the typical level of accuracy which was achieved with the China Lake test series. The next section takes a broader look at the results for the test series as a whole.

5.3.2 China Lake Test Series- Overall Comparison Between the Modeling Results and Test Results

Predictions were made for 14 of the China Lake tests in which the data collected and the propellant characterization allowed rational comparisons with the model. Several key variables were used to characterize the overall performance of the predictions; the peak temperature, the temperature 60 seconds into the burn, the peak heat flux, and the heat flux at 60 seconds into the burn. The 60 second time is near the end of the propellant burn when Class A fuels are most likely to ignite. The top thermocouple of the vent tree was used to represent the hot layer temperature and the floor mounted upward facing total heat flux transducer was used to characterize the heat flux to the floor.

Overall, the difference between the predicted and measured peak temperatures is less than 200°C, and there is a tendency for the predictions to be somewhat less than the upper thermocouple in the vent tree. The average error in the peak temperature is -78°C (i.e., underpredicted) and the standard deviation, σ^2, is 89°C. As Figure 6 indicates, the upper vent tree thermocouple is somewhat higher than the overall average of all thermocouples in the upper half of the compartment. As a result, the tendency to underpredict is expected. Similarly, the temperature predictions at 60 seconds into the burn are generally underpredicted with the average error -94°C (σ^2=128°C). Here again, the upper vent tree thermocouple is systematically higher than the average of the thermocouples in the upper half of the compartment.

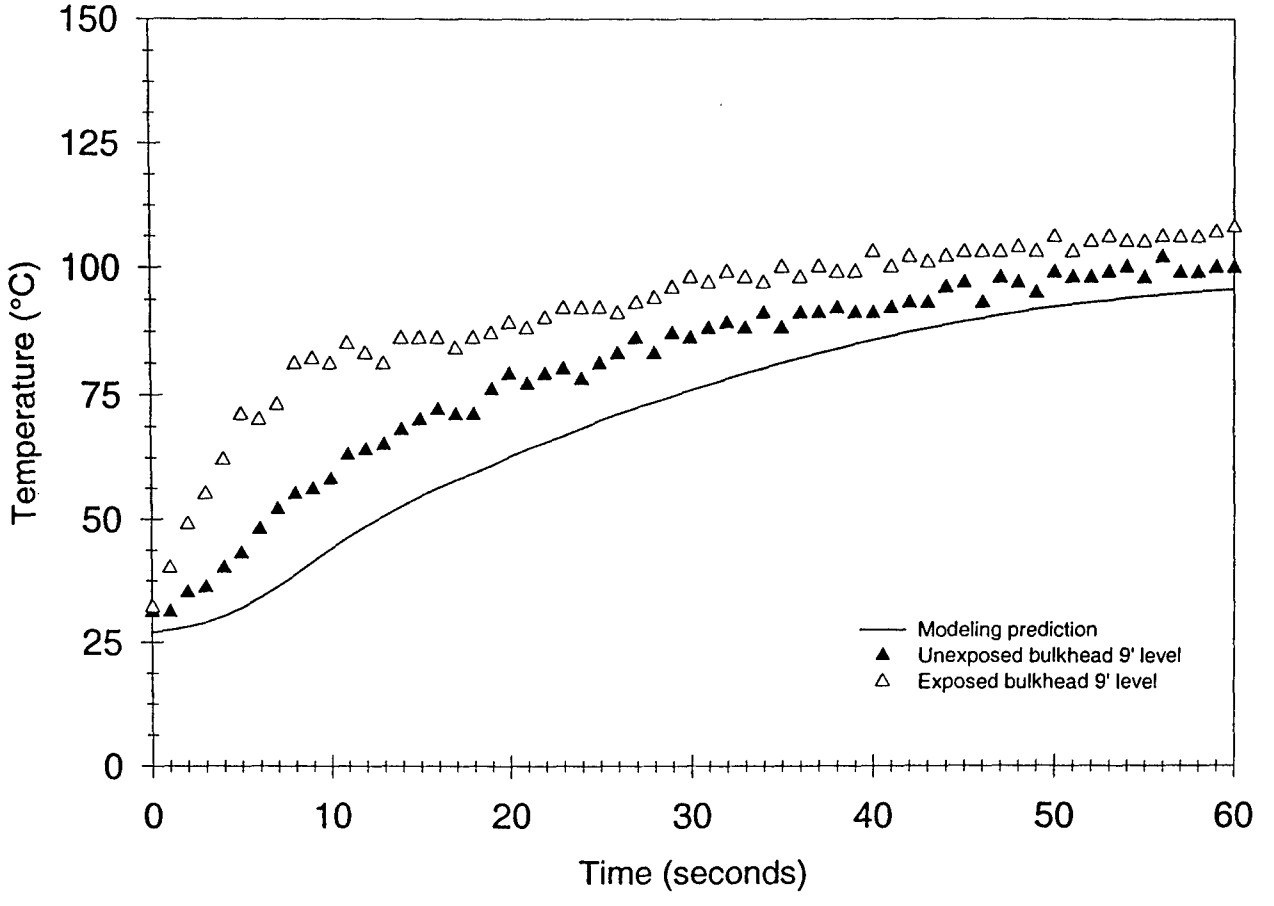

Figure 7 – Modeling prediction compared to China Lake, Test 20, wall temperature

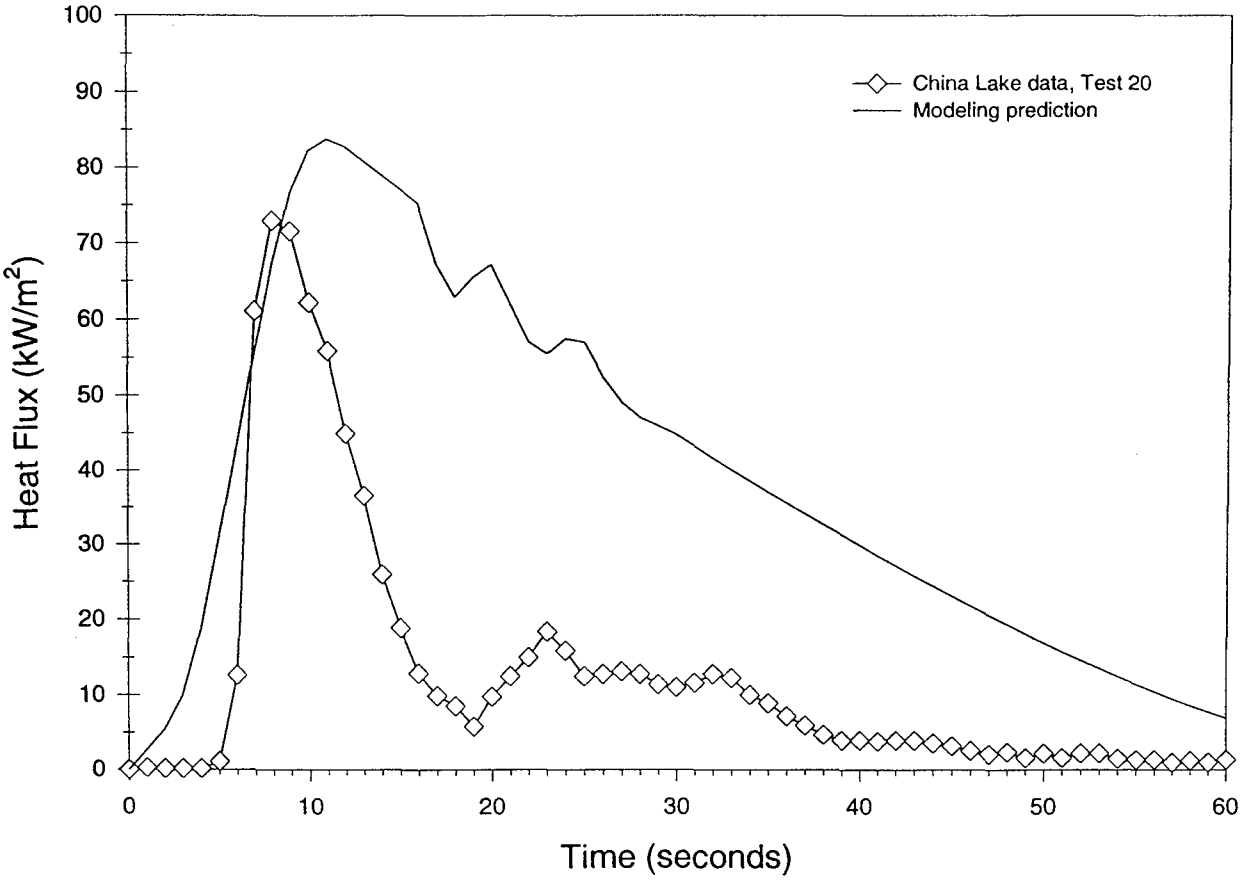

Figure 8 – Modeling prediction of heat flux at floor level as compared with China Lake data for Test 20

The average error in the predicted peak radiative heat flux is 32 kW/m^2 (overpredicted) with a standard deviation of 25 kW/m^2. Unlike the temperature predictions, the heat fluxes are overpredicted. Similar results are observed in the predictions of radiative heat flux made 60 seconds into the burn. The average error in the heat flux at 60 seconds is 6.2 kW/m^2 (overpredicted) and the standard deviation is 3.7 kW/m^2. These are significant overpredictions since the average observed flux is around 2 kW/m^2. The experimental data are thought to be low due to significant aluminum oxide (Al_2O_3) deposition on the upward facing transducer surface. The thermal performance benchmarks have been summarized in Table 1.

Table 1. Thermal Performance of Fire Model for Missile Propellant Simulations

Variable	Baseline Comparison Predictions China Lake Test Series	
	Average Error†	Standard Deviation
Peak Temperature (°C)	-78	89
Temperature at 60s (°C)	-94	128
Peak Heat Flux (kW/m^2)	32	25
Heat Flux at 60s (kW/m^2)	6.2	3.7

†Errors are the (predicted value - observed value), i.e., positive errors are over predictions.

6.0 HULVUL TEST DESCRIPTION

The HULVUL test series was conducted on an ex-LEANDER-Class Royal Navy frigate. The model was then exercised to blindly predict the experiments performed in the HULVUL test series. The compartment testing configuration, ventilation arrangements, instrumentation and fuel configuration have been described for both the HULVUL tests series in Reference 3 and are presented in the following section.

6.1 HULVUL Shipboard Test Configuration

The HULVUL test series was executed on a ex-LEANDER Class Frigate. Several modifications were made to the ship prior to the tests. The propellant burns occurred in the Junior Ratings Dining Hall, which is located directly below the flight deck. The combustible contents and all combustible bulkhead/overhead treatments were stripped from the burn compartment and from the burn compartment's unexposed surfaces in adjacent compartments. A ventilation opening was cut into the hull measuring 2.0 m (6.8 ft) wide by 1.7 m (5.8 ft) tall. Two steel compartments 2.4 x 2.4 x 2.4 m (8 x 8 x 8 ft) were fabricated on the flight deck above the burn compartment to

simulate vertically adjacent compartments. Figure 9 shows a section view of the compartments used in the tests.

The HULVUL burn compartment volume was 100 m^3 (3500 ft^3), slightly smaller than the China Lake 114 m^3 (4000 ft^3) compartment. The notable differences between the two burn compartments are as follows:

- The HULVUL burn compartment height was 2.28 m (7.6 ft), compared with the China Lake 3.05 m (10 ft) compartment height;
- The HULVUL burn compartment was rectangular (approximately 7.6 m x 5.2 m (25 ft x 17 ft)), compared with the square China Lake compartment 6.1 m x 6.1 m (20 ft x 20 ft); and
- The HULVUL burn compartment had 0.32 cm (⅛ in.) bulkheads and 0.48 cm (3.16 in.) decks, compared with the China Lake simulated shipboard compartments which utilized 0.96 cm (0.375 in.) thick bulkheads and 1.27 cm (½ in.) thick decks.

Several thermocouple trees were installed for the HULVUL tests. Each thermocouple tree consisted of eight thermocouples, each spaced 0.3 m (1 ft) apart starting at 15.2 cm (6 in.) above the deck to 15.2 cm (6 in.) below the overhead. A Type S high temperature thermocouple tree was installed 0.91 m (3 ft) from the location of the burning fuel in order to measure temperatures at or near the plume. Three Type K, 1.5 mm diameter inconel-sheathed thermocouple trees were installed forward, aft, and center of the burn compartment. Additionally, 0.4 mm diameter, bare bead, Type K thermocouple trees were installed in the following locations: one in the vent of the burn compartment; one in the passageway nook of the burn compartment; three in laterally adjacent compartments (one each in the Galley, Power Room, and PO Mess) and one in each of the two deck houses. Thermocouple locations as well as the additional instrumentation are shown in Figure 10.

Each of the adjacent compartments have a heat flux transducer and a radiometer installed 0.31 m (1 ft) away from the bulkhead which is in common with the burn compartment. Radiometers were installed at the fuel height elevation, facing the missile propellant at distances of 1.5 m (5 ft), 3.1 m (10 ft) and 4.5 m (15 ft) from the fuel pan. There was an additional total heat flux transducer installed along with the radiometer at the 4.5 m (15 ft) distance directly facing the fuel pan. All heat flux transducers and radiometers were water cooled and the radiometers included 150 degree sapphire windows.

The pressure transducers were installed to monitor the pressure increase in the burn compartment which corresponds to the rapid thermal expansion of gases. Two optical thermocouples/infrared pyrometers (spectral range: 1-2.5 microns) were installed to measure the temperature of the plume and the fuel surface during the test.

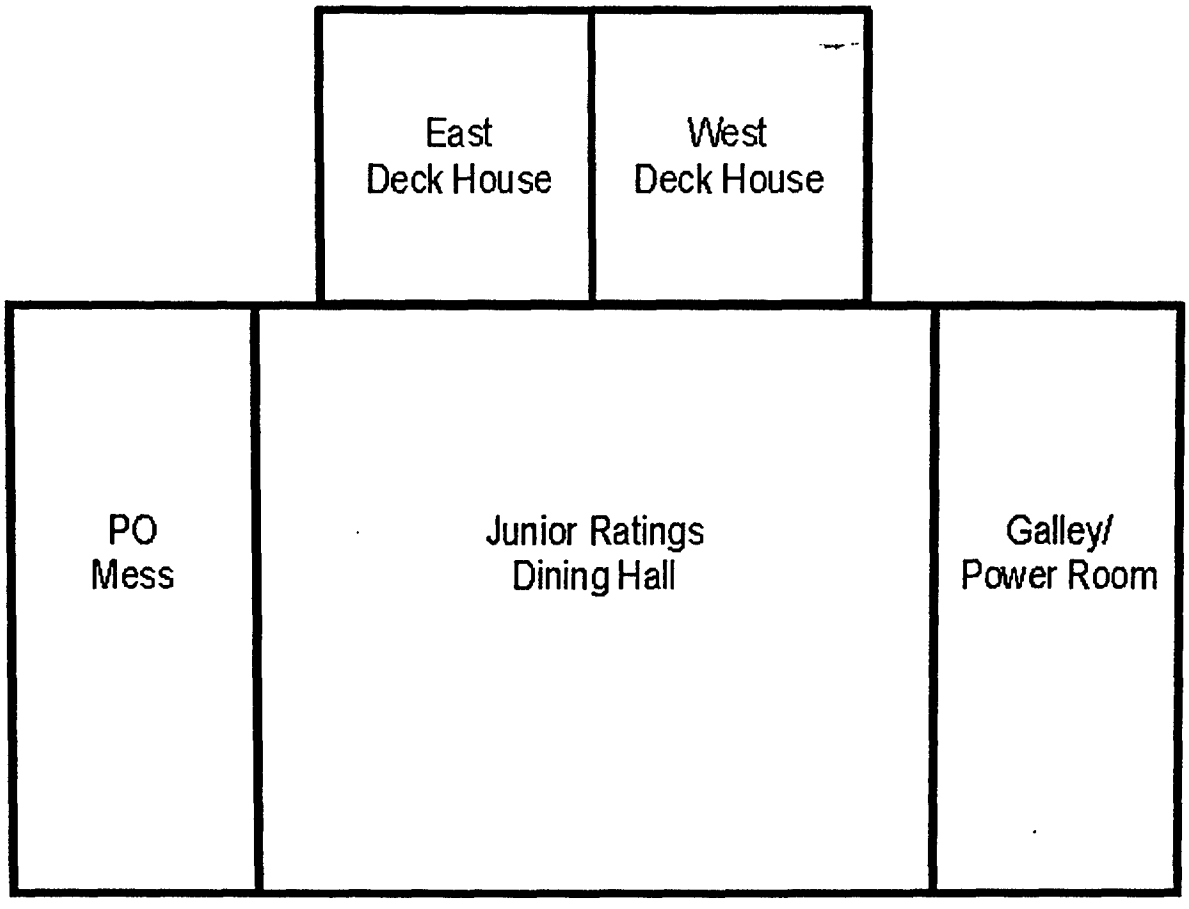

Figure 9 – Section vies of test area on the ex-LEANDER Class Frigate

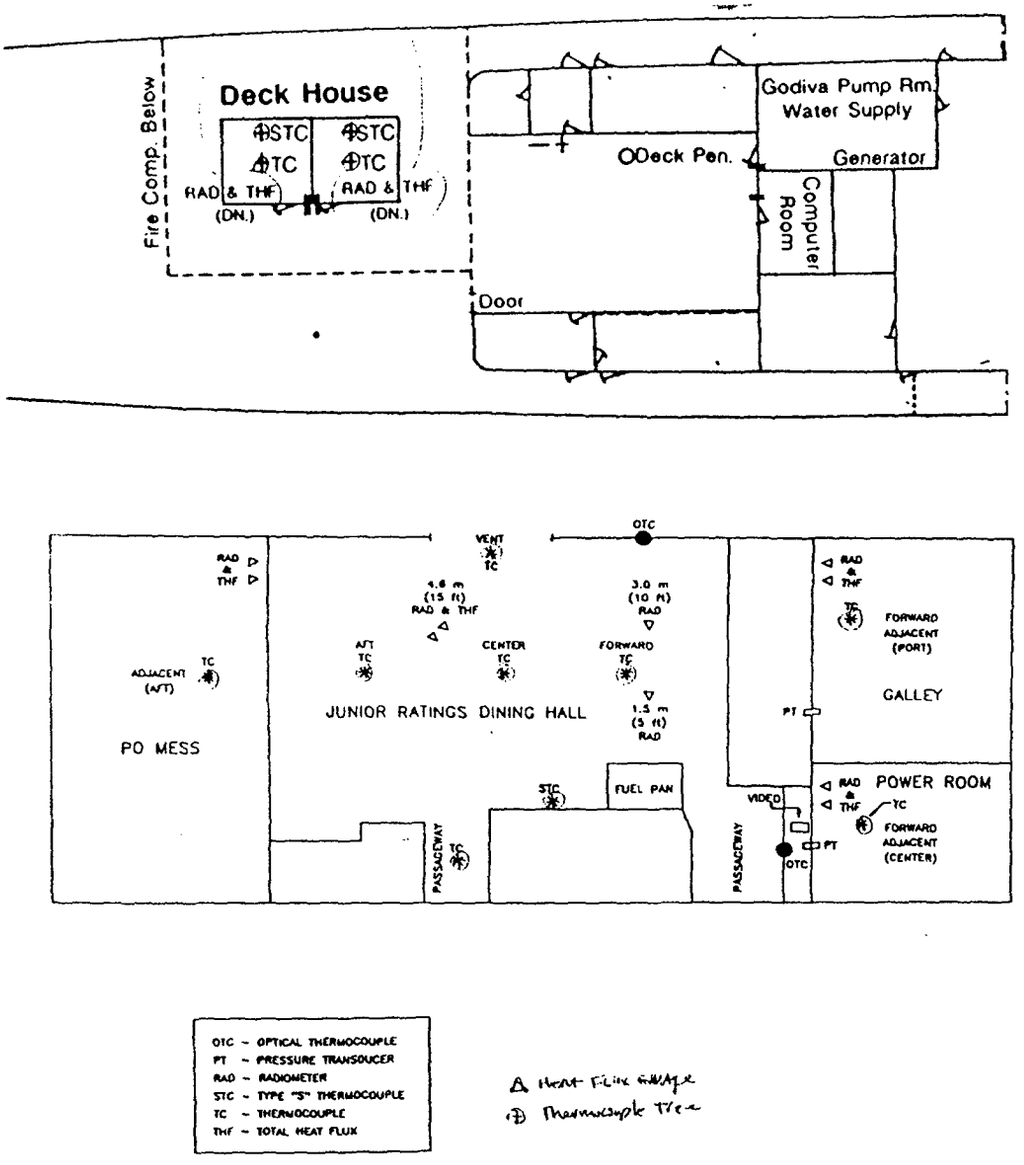

Figure 10 – HULVUL test series instrumentation layout

6.2 HULVUL Test Series

Twelve propellant burn tests were conducted on the HULVUL test ship. Four tests were baseline tests, five investigated vent size effects and three incorporated large wood cribs to evaluate ignition of Class A materials. All twelve of these tests were blindly predicted. Varying amounts of missile propellant were used and included 22.7, 45.3, 68.0, and 90.1 kilogram quantities (50, 100, 150, and 200 lbs), while the most prevalent size was 68.0 kg (150 lbs), which was used in seven of the tests. Vent sizes included a range of openings: 1.4, 1.86, 2.32, 2.79, and 3.56 square meters (15, 20, 25, 30, and 38.3 ft^2), created by adjusting the width of the vent opening and maintaining a vent height of 1.7 m (5.8 ft).

6.3 HULVUL Test Series - Comparison of Modeling Results with Test Results

All twelve of the HULVUL tests were predicted without prior knowledge of the test results. The full comparison of all twelve tests is included as Appendix A. The inputs were determined from the compartment characteristics and the mass and shape of the propellant charge used in the test. As with the China Lake tests, several key variables can be used to characterize the overall performance of the predictions. Errors in the predictions of the peak temperature, the temperature 60 seconds into the burn, the peak heat flux, and the heat flux at 60 seconds into the burn are shown in Table 2 and discussed in this section.

Table 2. Thermal Performance of Fire Model for Missile Propellant Simulations

Variable	Baseline Comparison Predictions China Lake Test Series		Blind Predictions - HULVUL Test Series	
	Average Error†	Standard Deviation	Average Error†	Standard Deviation
Peak Temperature (°C)	-78	89	8	42
Temperature at 60s (°C)	-94	128	-62	68
Peak Heat Flux (kW/m^2)	32	25	3	39
Heat Flux at 60s (kW/m^2)	6.2	3.7	-2.2	2.0

†Errors are the (predicted value - observed value), i.e., positive errors are over predictions.

Predicted peak temperatures in the HULVUL series were generally in excellent agreement with the test results, with an average error of 8°C and a standard deviation of σ^2=42°C for eleven of the twelve tests. The twelfth test was overpredicted by 373°C. An examination of the test data for that test indicates that there was difficulty getting complete ignition of the entire fuel package. The results of Test 12 are not included in any performance statistics. The predicted layer

temperatures at 60 seconds are generally somewhat low with an average error of -62°C and a standard deviation of 68°C.

The average error for the peak heat flux is 3 kW/m^2 with a standard deviation σ^2=39 kW/m^2. In most tests the peak flux is somewhat overpredicted though the two worst predictions are lower than the observed values from the test. The heat flux at 60 seconds was also generally underpredicted, with an average error of 2.2 kW/m^2 and a standard deviation of σ^2=20 kW/m^2. This trend is consistent with the predictions of the layer temperature and is significantly better than in the China Lake tests. In the HULVUL tests the total heat flux transducer (located 15 ft from the fuel at floor level) was facing the burning propellant rather than facing upward as it had in the China Lake tests. This configuration limited the aluminum oxide (Al_2O_3) buildup on the transducer.

Results from three tests have been presented as a sample of the blind HULVUL test/modeling comparisons. HULVUL Tests No. 2, No. 3, and No. 4 investigated three different fuel loads given a 2.79 m^2 (30 ft^2) vent opening. The missile propellant fuel loads of 45.3 kg, 68.0 kg, and 90.1 kg (100, 150, and 200 lb) were ignited in HULVUL Test No. 2, No. 3, and No. 4 respectively. Figures 11 through 13 depict the compartment temperature predictions compared with the data for each of these three HULVUL tests. Figures 14 through 16 illustrate the floor level heat flux predictions compared with the test data for each of these three HULVUL tests. These figures give a sense for the level of agreement between the modeling predictions and the test data for blind simulations over a range of missile propellant fuel package sizes.

7.0 SUMMARY OF MODELING PERFORMANCE

Table 2 summarizes the thermal performance of the model in predicting both test series. The improved performance of the model in the HULVUL series can be attributed both to improvements in modeling and the experiments. It was observed in the China Lake series that the quality of the data improved as the series continued. This trend appears to have continued into the HULVUL series. Further, all the fuel elements were better characterized in the HULVUL series than in some of the China Lake series. This improved characterization of the fuel loads resulted in better model inputs and hence model performance. Finally, the burning rate algorithm used to estimate the burning rate in the HULVUL predictions was more sophisticated than that used in the China Lake test series.

The model predicts the conditions in the compartment away from the propellant source. The effects of direct radiation from the propellant to other fuels are not included, and the effect of direct impingement of the propellant plume is not modeled.

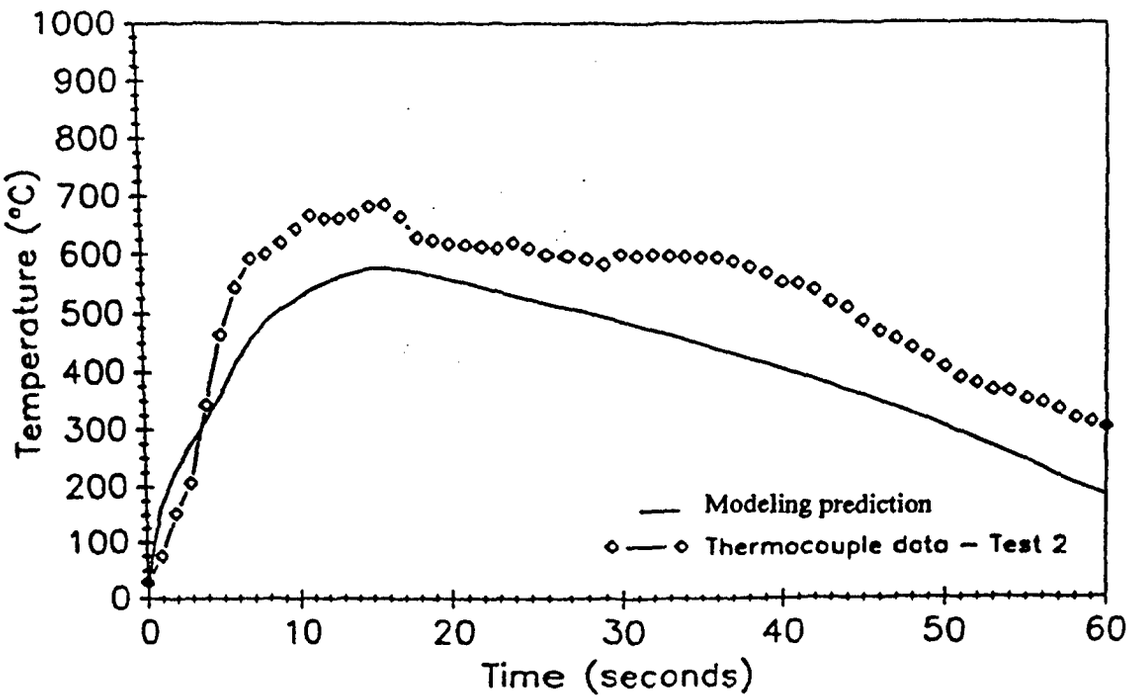

Figures 11 – Modeling prediction compared to HULVUL, Test 2, upper layer

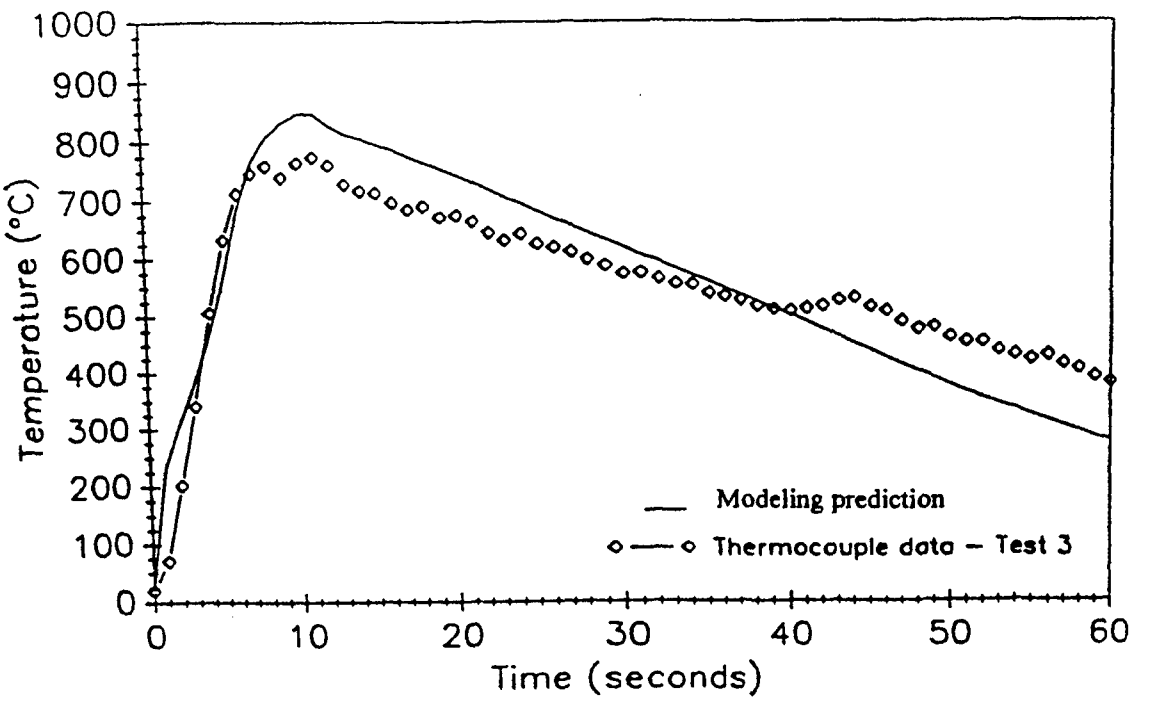

Figure 12 – Modeling prediction compared to HULVUL, Test 3, upper layer temperature

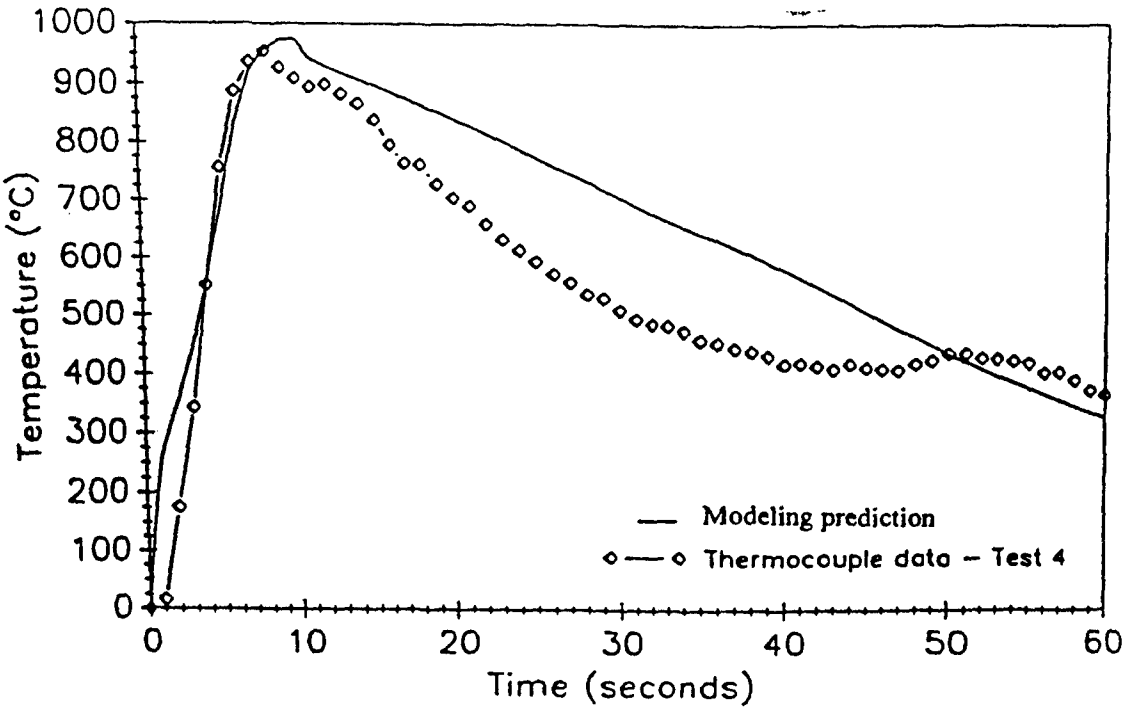

Figure 13 – Modeling prediction compared to HULVUL, Test 4, upper layer temperature

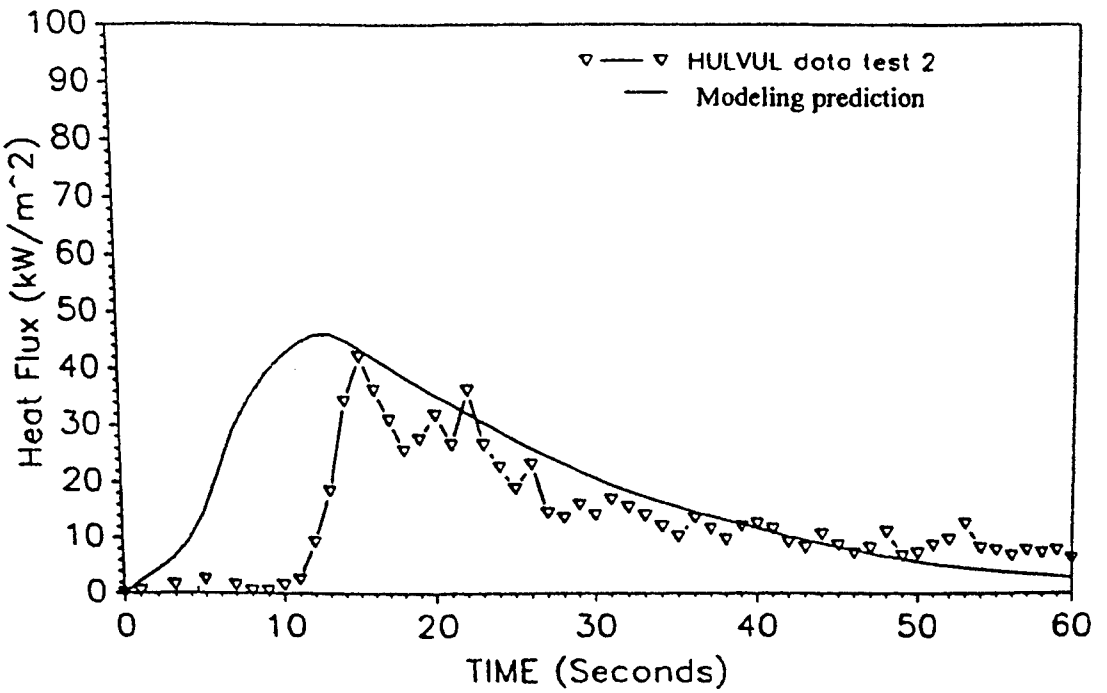

Figure 14 – Modeling prediction of heat flux at floor level as compared with HULVUL data for Test 2

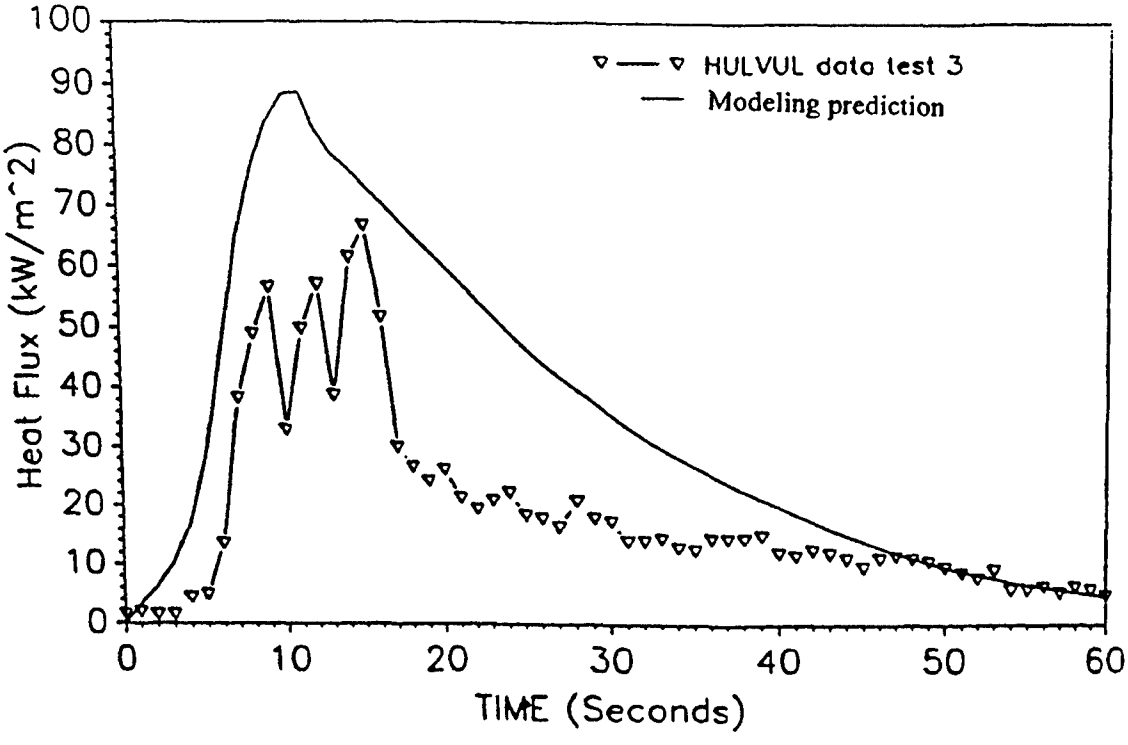

Figure 15 – Modeling prediction of heat flux at floor level as compared with the HULVUL data for Test 3

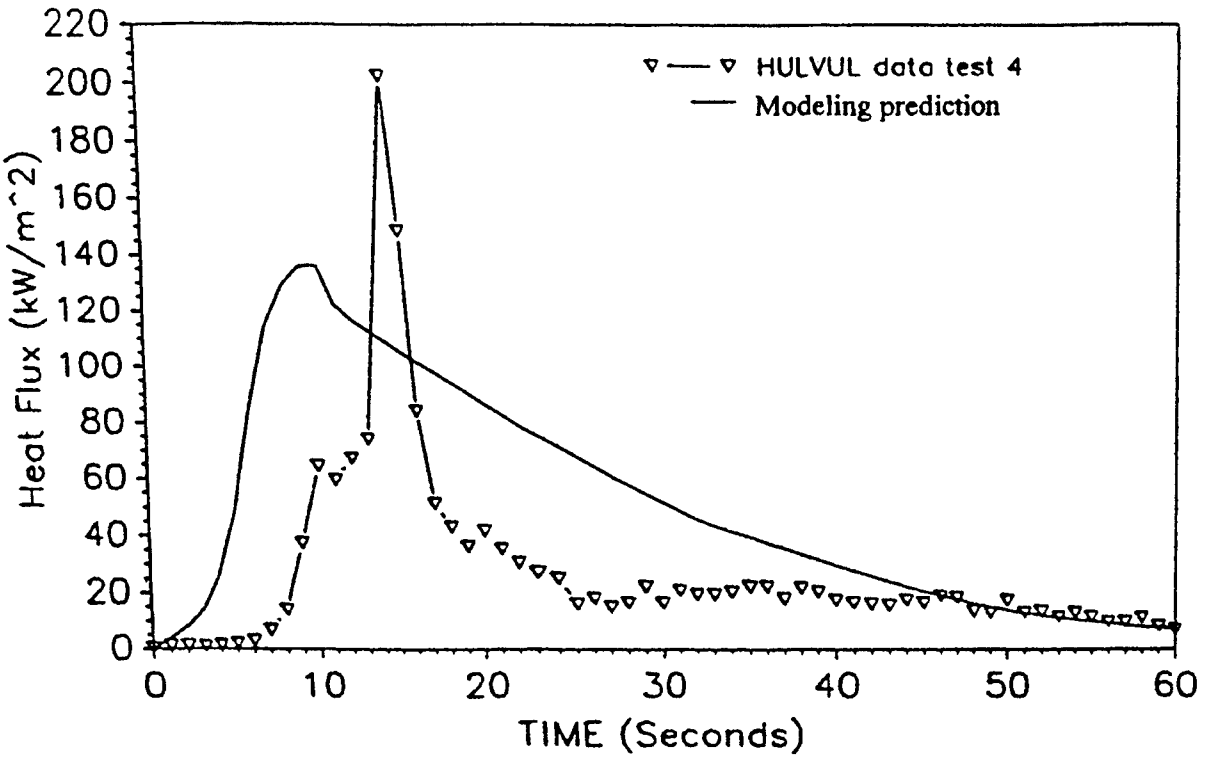

Figure 16 – Modeling prediction of heat flux at floor level as compared with HULVUL data for Test 4

The comparisons of model predictions and experimental results in the China Lake and HULVUL test series show that the model provides good estimates of the environment created by propellant burning in a ship compartment. The predicted heat flux histories and compartment conditions can be used, in conjunction with oxygen concentration predictions or characterizations, to predict whether Class A materials will be ignited. Conservative assessments would assume sufficient oxygen for ignition of thermally thin Class A materials with low elevations and in close proximity to the vent. FAST could be modified in the future to allow the unconstrained burning of the missile propellant while simultaneously tracking the oxygen content in the compartment. This was not pursued in the scope of the reported effort. The current CFAST model still does not include oxygen predictions in unconstrained fires nor does it allow mixing constrained and unconstrained fires for different items in the same simulation. This limits the ability to model both the propellant burn and the subsequent burning of ordinary combustibles.

7.1 Notation

A	surface area of the missile propellant (m^2)
C	constant in missile propellent regression rate
L	length of cylindrical missile propellant element (m)
L_o	initial length of missile propellant fuel package (m)
$\dot{m}$	mass burning rate of missile propellant (kg/s)
$\dot{m}_o$	initial burning rate of the missile propellant fuel package (kg/s)
P	pressure of environment where propellant combustion takes place (atm)
R	radius of cylindrical missile propellant element (m)
R_o	initial radius of missile propellant fuel package (m)
t	elapsed burning time (s)
t_b	total burning duration (s)
V	linear regression rate associated with missile propellant combustion

Greek Symbol

ρ	density (Us/m^3)

8.0 REFERENCES

1. "Qualification of Thermal Insult from Residual Missile Fuel," Hughes Associates, Inc., Baltimore, MD, April 1990.

2. Farmer, K.R., Bowman, H.L., Leonard, J.T., Darwin, R.L., and Burns, R.E., "Thermal Environments Generated by Combustion of Solid Rock Propellant In Shipboard Compartments," NAWCWPNS TP 8097, Naval Air Warfare Center Weapons Division, China Lake, CA, December 1993.

3. Leonard, J.T., Fulper, C.R., Darwin, R.L., Farmer, K.R., Boyer, L., Burns, R.E., Back, G.G., Hayes, E.D., and Ouellette, R.J., "Project HULVUL: Propellant Fires in a Shipboard Compartment," NRL Report 9363, Naval Research Laboratory, Washington, DC, November 29, 1991.

4. Back, G.G., Darwin, R.L., Scheffey, J.L., and Williams, F.W., "Propellant Fires in a Simulated Shipboard Compartment: Project HULVUL - Phase III," NRL Report NRL/MR/6180-99-8394, Naval Research Laboratory, Washington, DC, August 20, 1999.

5. Mitler, H., and Rockett, J., "User' Guide to FIRST, A Comprehensive Single-Room Fire Model," NBSIR 87-3595, National Bureau of Standards, Gaithersburg, MD, 1987.

6. Jones, W., and Peacock, R., "Technical Reference Guide for FAST Version 18," NIST Technical Note 1262, National Institute for Standards and Technology, Gaithersburg, MD, 1989.

7. Bukowski, R., Peacock, R., Jones, W., and Forney, L., "Hazard I Fire Hazard Assessment Model," NIST Handbook 146, National Institute for Standards and Technology, Gaithersburg, MD, 1989.

8. Cooper, L.Y., and Forney, G.P., "Fire in a Room with a Hole: Application of the Consolidated Compartment Fire Model (CCFM) Computer Code," 1987 Eastern States Combustion Institute Meeting, The Combustion Institute, Philadelphia, PA, 1987.

9. Mitler, H., and Emmons, H., "Documentation for CFC V, The Fifth Harvard Computer Fire Code," NBS-GCR-81-344, National Bureau of Standards, Gaithersburg, MD, 1981.

10. Lee, S.C., and Tien, C.L., *Progress in Energy and Comb. Sci.*, **8**, 41, 1982.

11. Timnat, Y.M., *"Advanced Rocket Propulsion,"* Academic Press, London, 1987.

APPENDIX A
Comparisons of Model Predictions with the HULVUL Test Series

This appendix includes comparisons of temperature and heat flux for all twelve of the HULVUL tests as well presentations of the calculated interface locations.

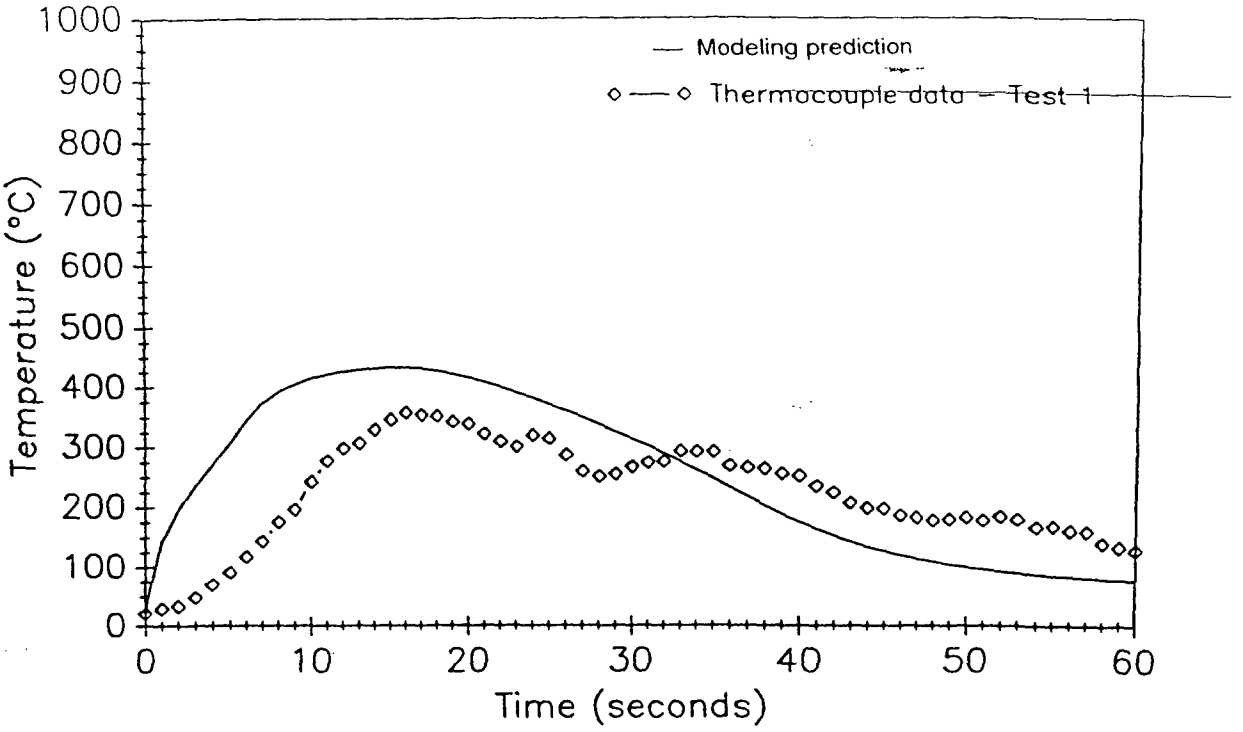

Figure A - 1. Modeling prediction compared to HULVUL data for Test 1, upper layer temperature

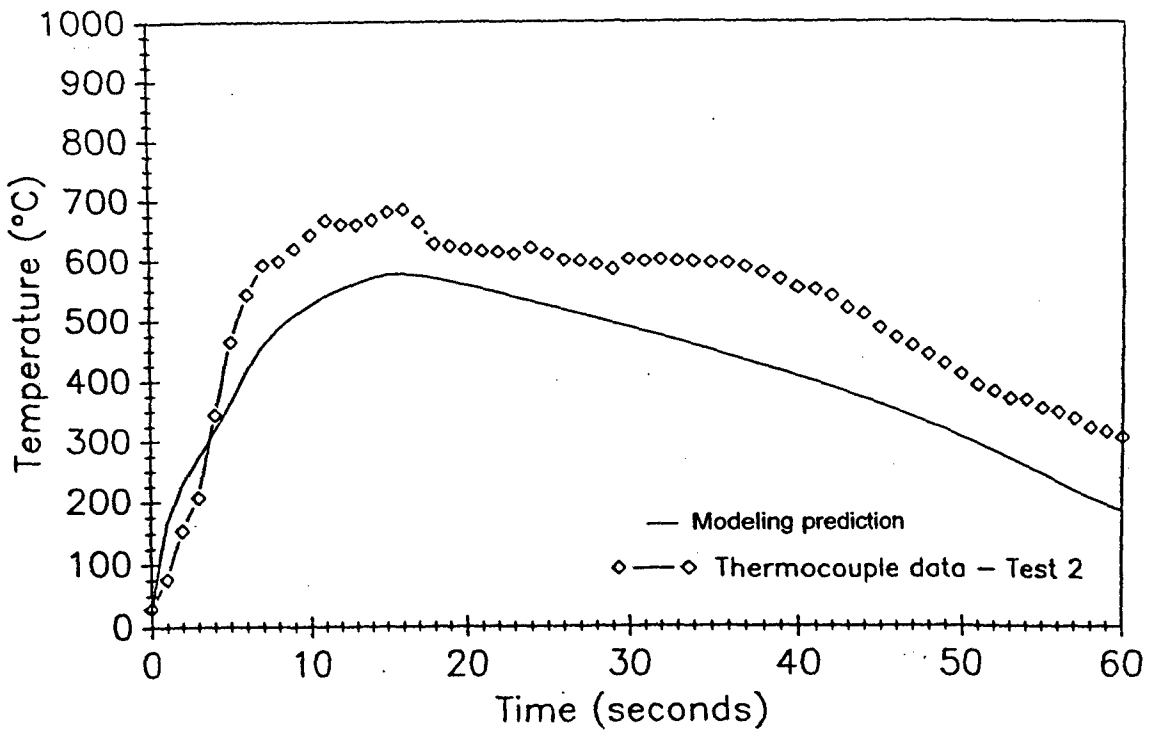

Figure A - 2. Modeling prediction compared to HULVUL data for Test 2, upper layer temperature

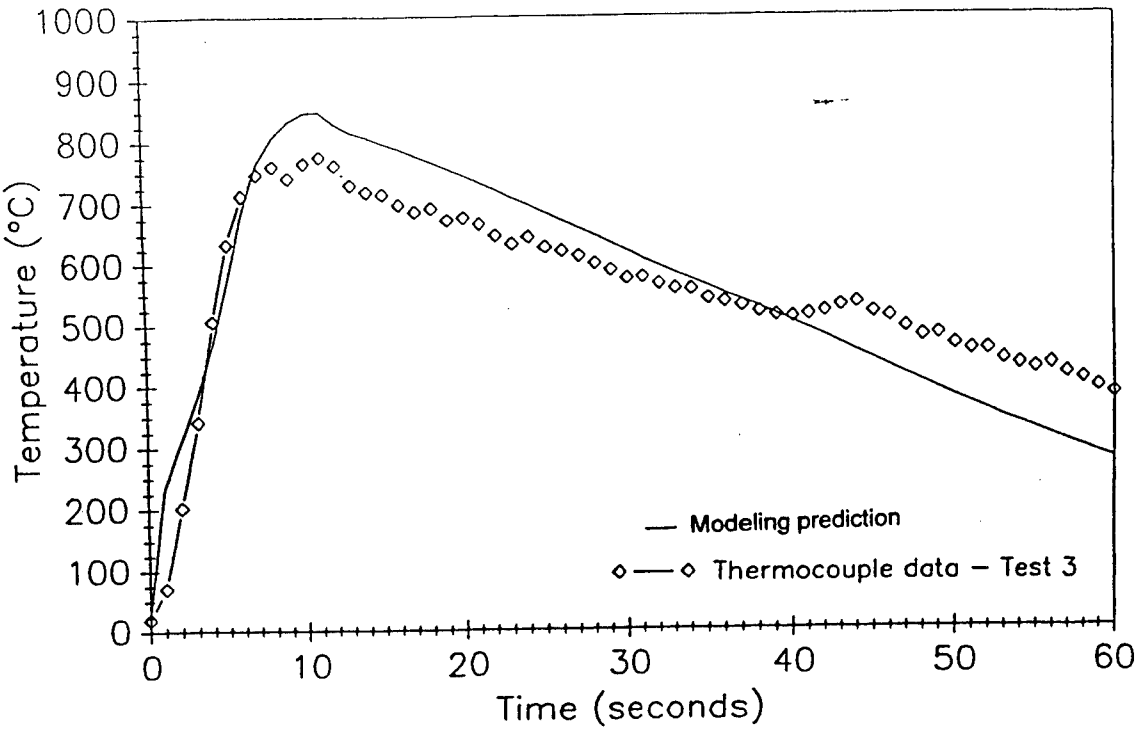

Figure A - 3. Modeling prediction compared to HULVUL data for TEST 3, upper layer temperature

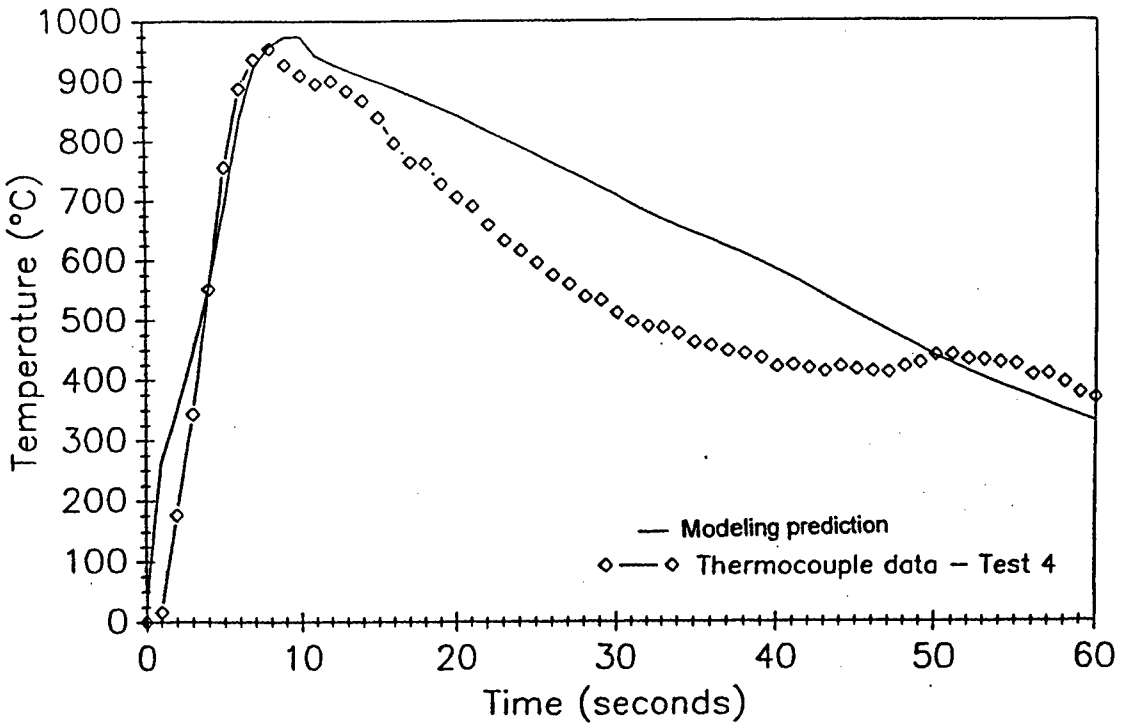

Figure A - 4. Modeling prediction compared to HULVUL data for Test 4, upper layer temperature

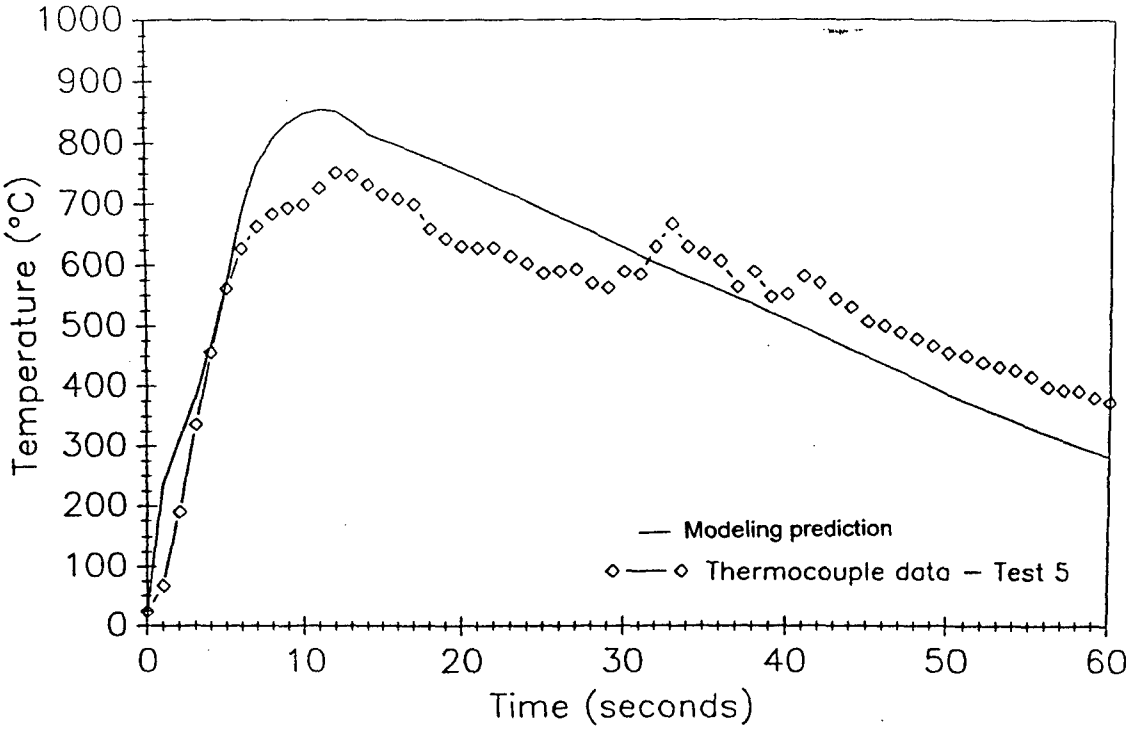

Figure A - 5. Modeling prediction compared to HULVUL data for Test 5, upper layer temperature

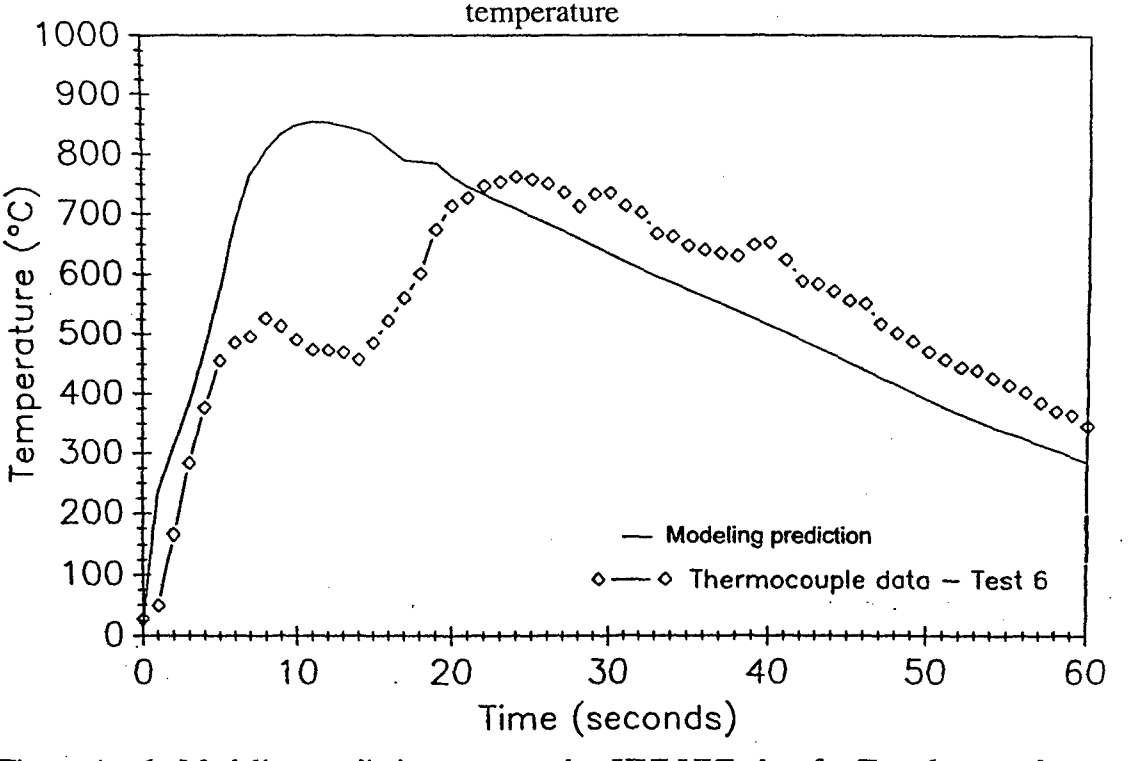

Figure A - 6. Modeling prediction compared to HULVUL data for Test 6, upper layer temperature

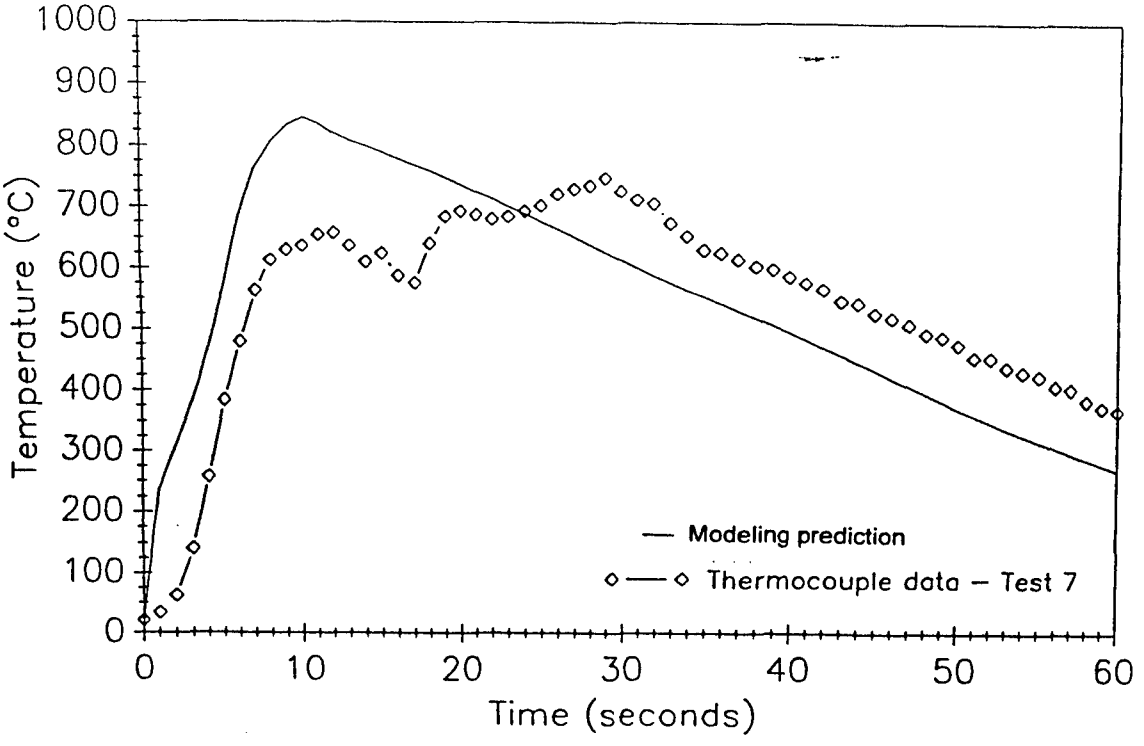

Figure A - 7. Modeling prediction compared to HULVUL data for Test 7, upper layer temperature

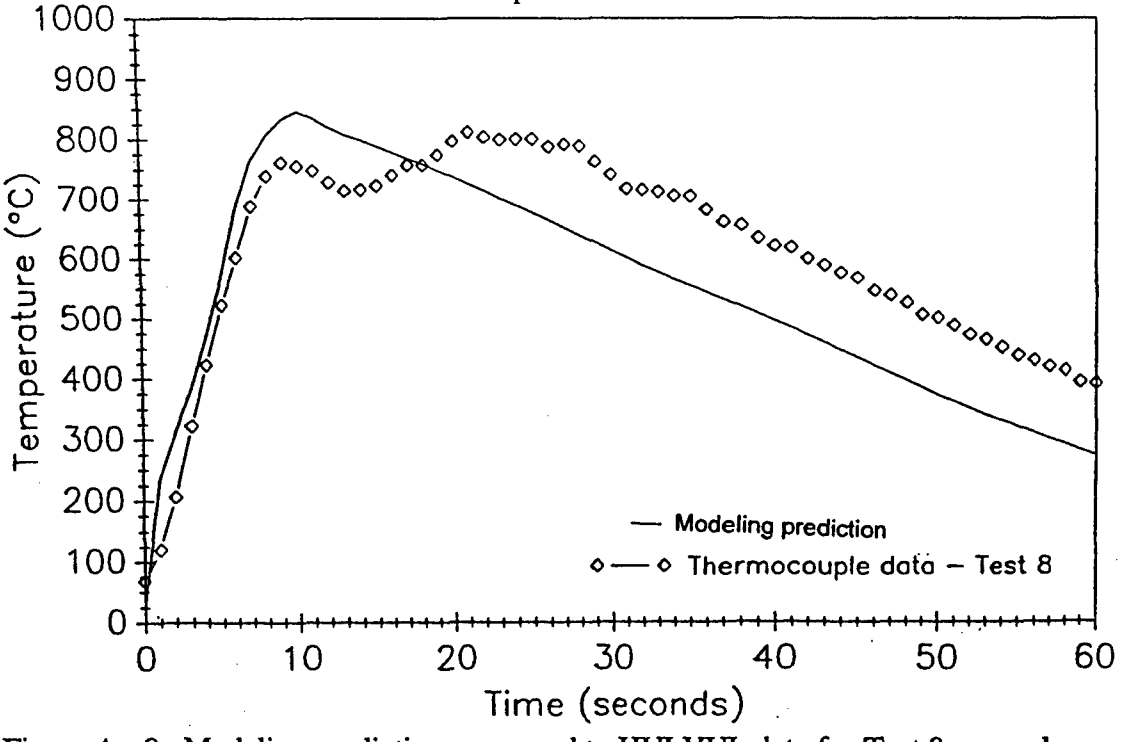

Figure A - 8. Modeling prediction compared to HULVUL data for Test 8, upper layer temperature

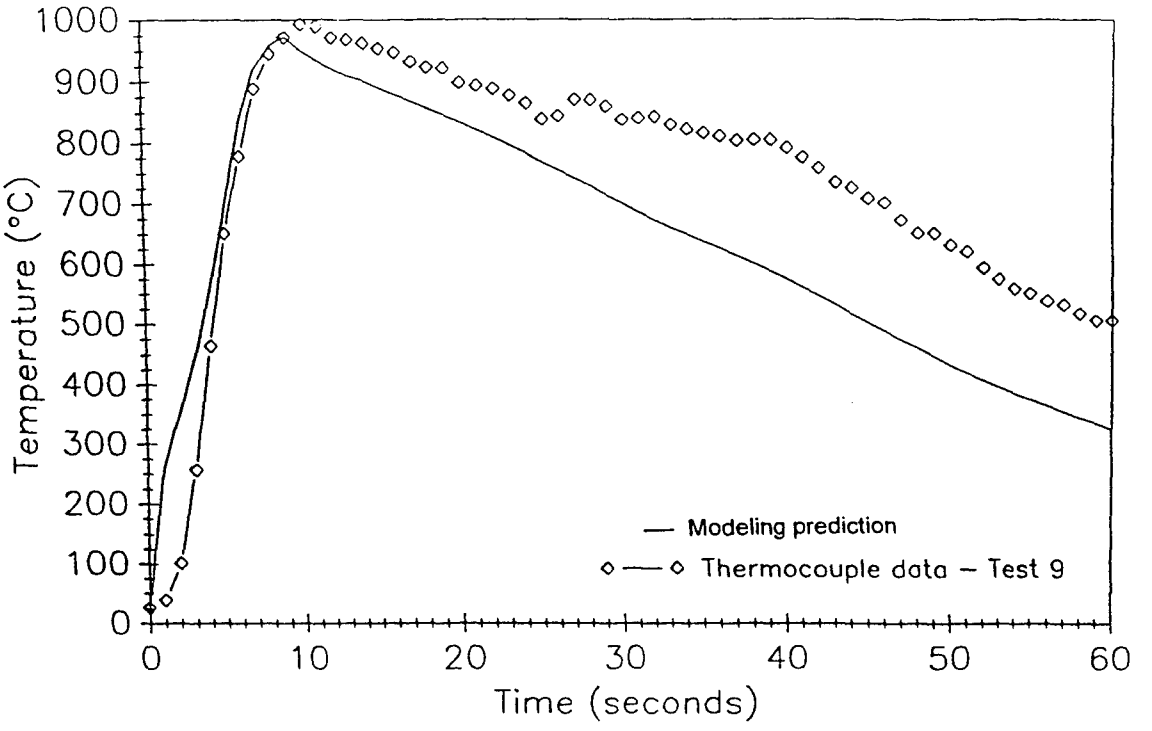

Figure A - 9. Modeling prediction compared to HULVUL data Test 9, upper layer temperature

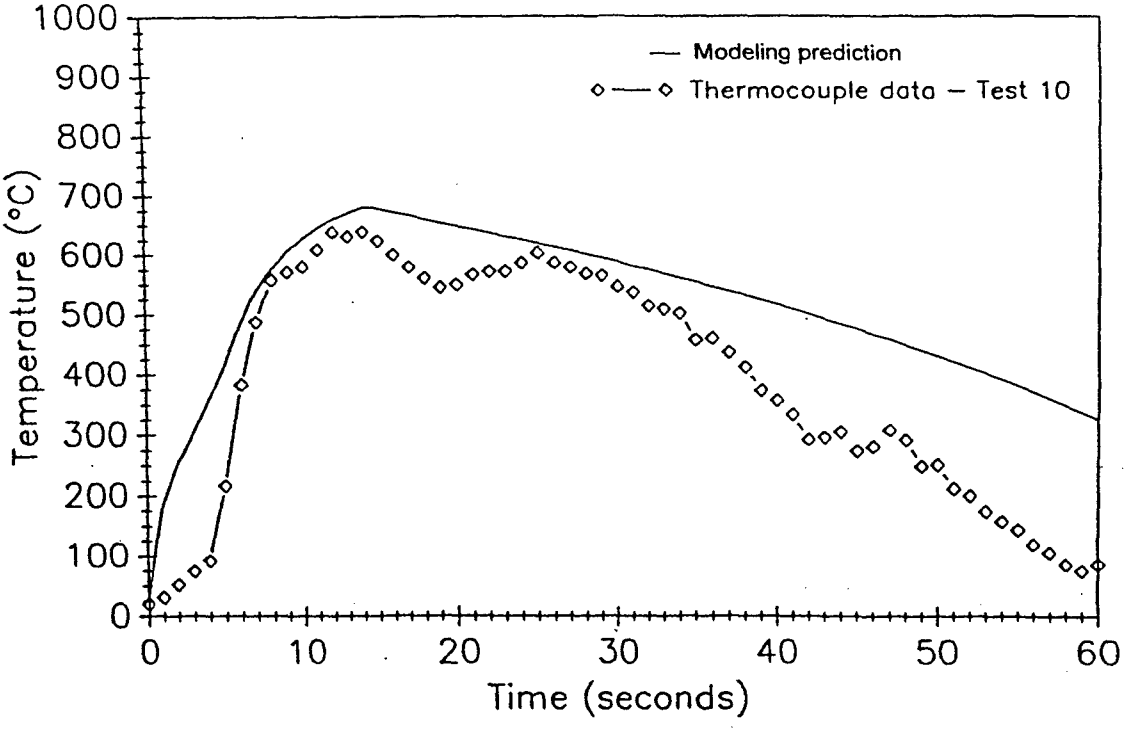

Figure A - 10. Modeling prediction compared to HULVUL data for Test 10, upper layer temperature

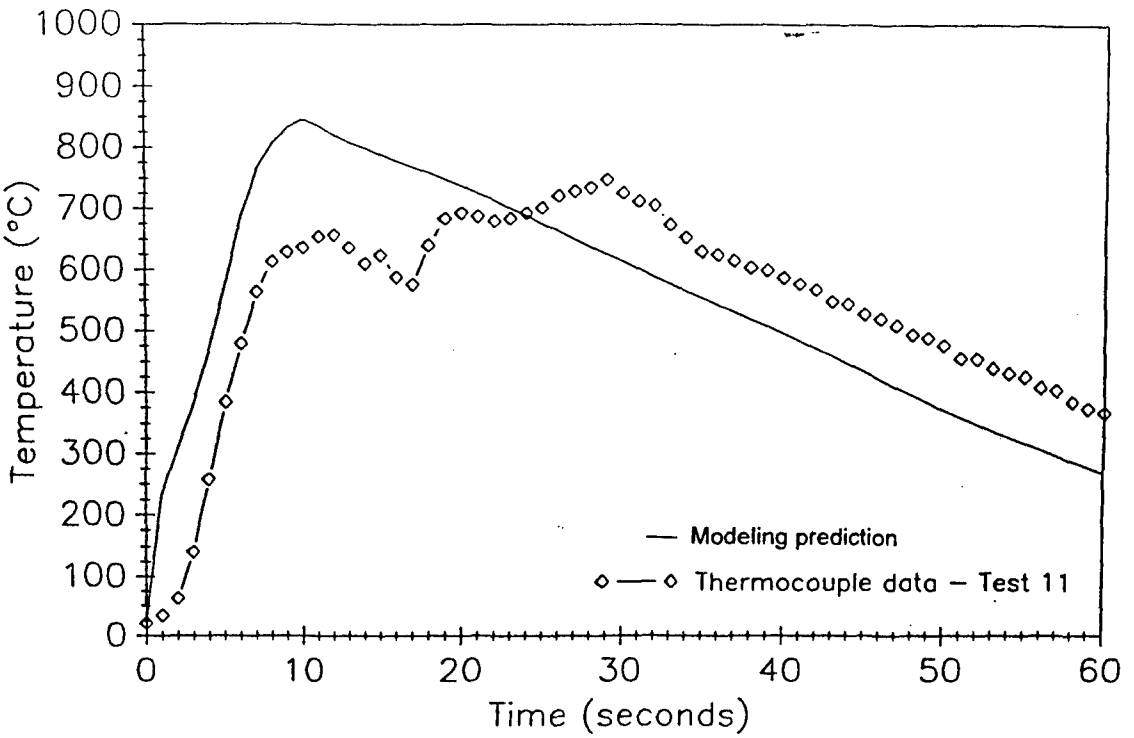

Figure A - 11. Modeling prediction compared to HULVUL data for Test 11, upper layer temperature

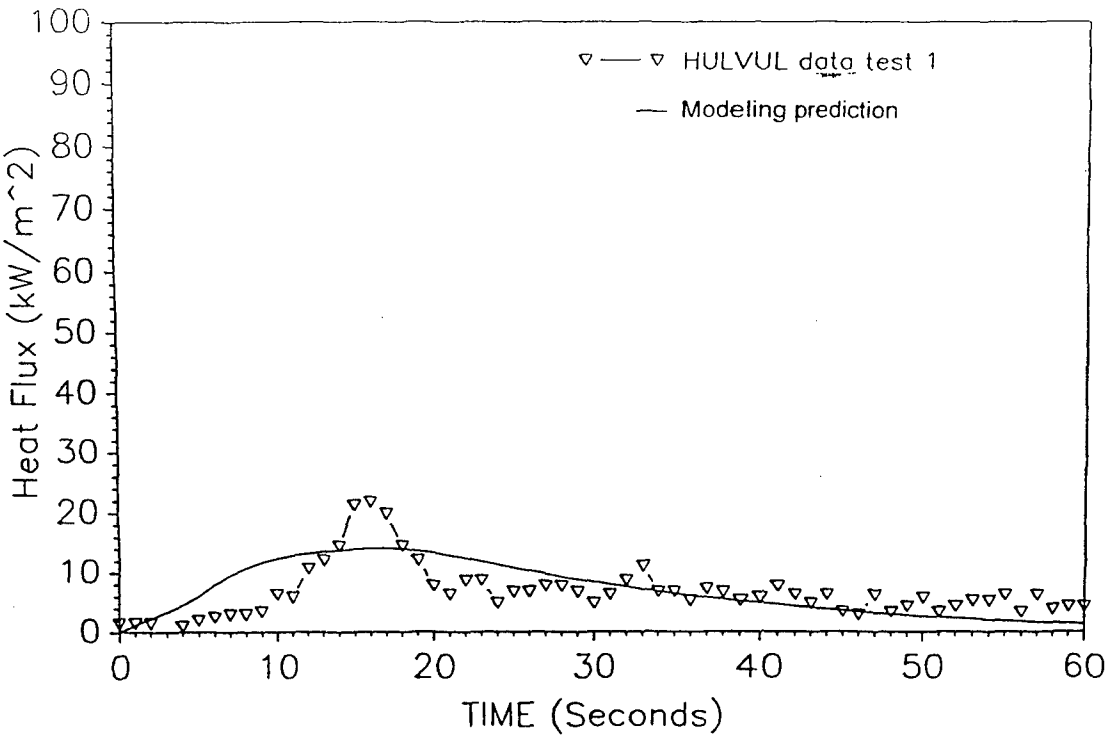

Figure A - 12. Modeling prediction of heat flux at floor level as compared with HULVUL data for Test 1

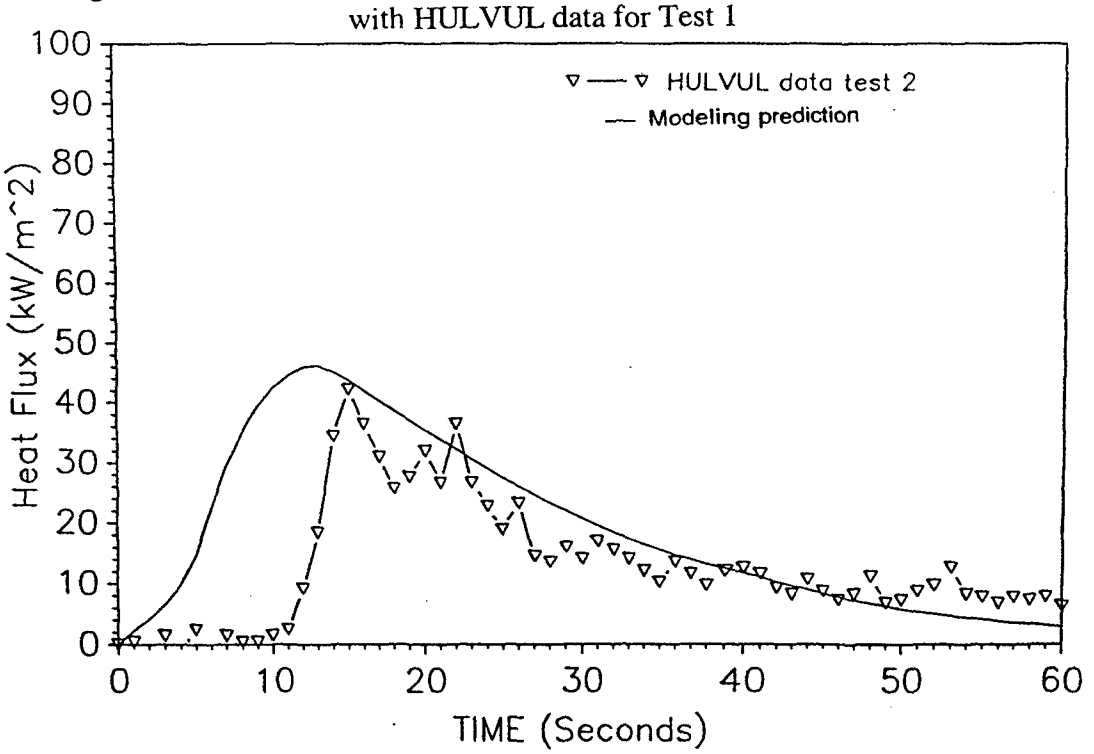

Figure A - 13. Modeling prediction of heat flux at floor level as compared with HULVUL data for Test 2

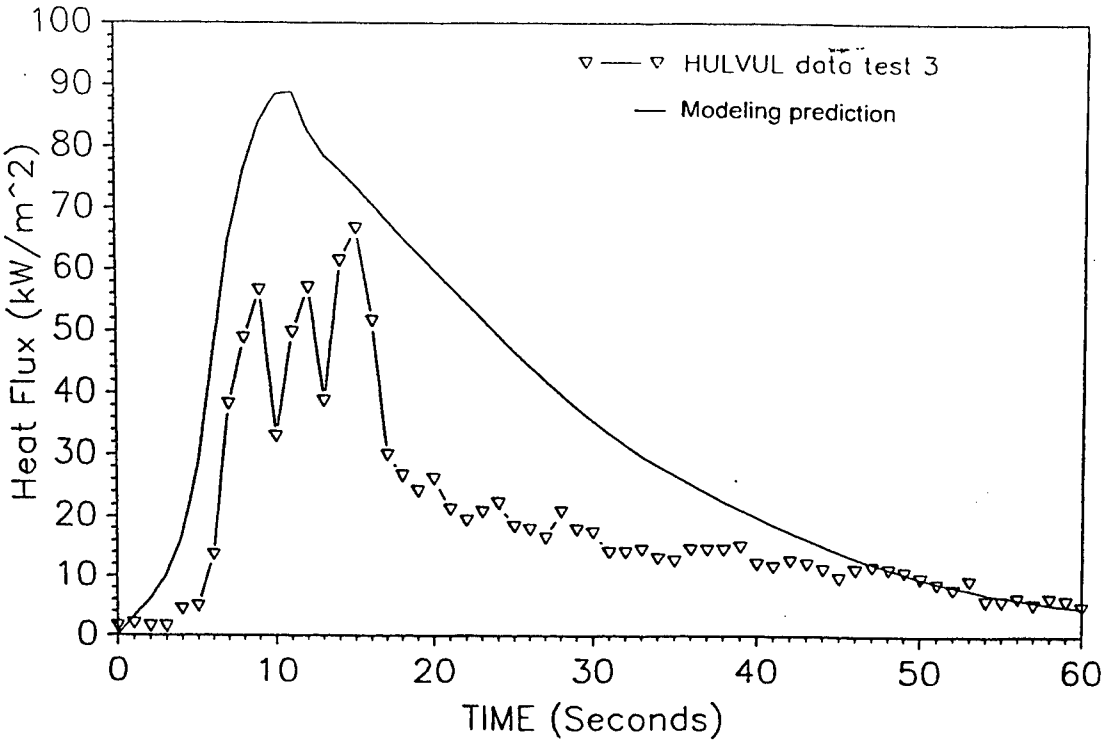

Figure A - 14. Modeling prediction of heat flux at floor level as compared with HULVUL data for Test 3

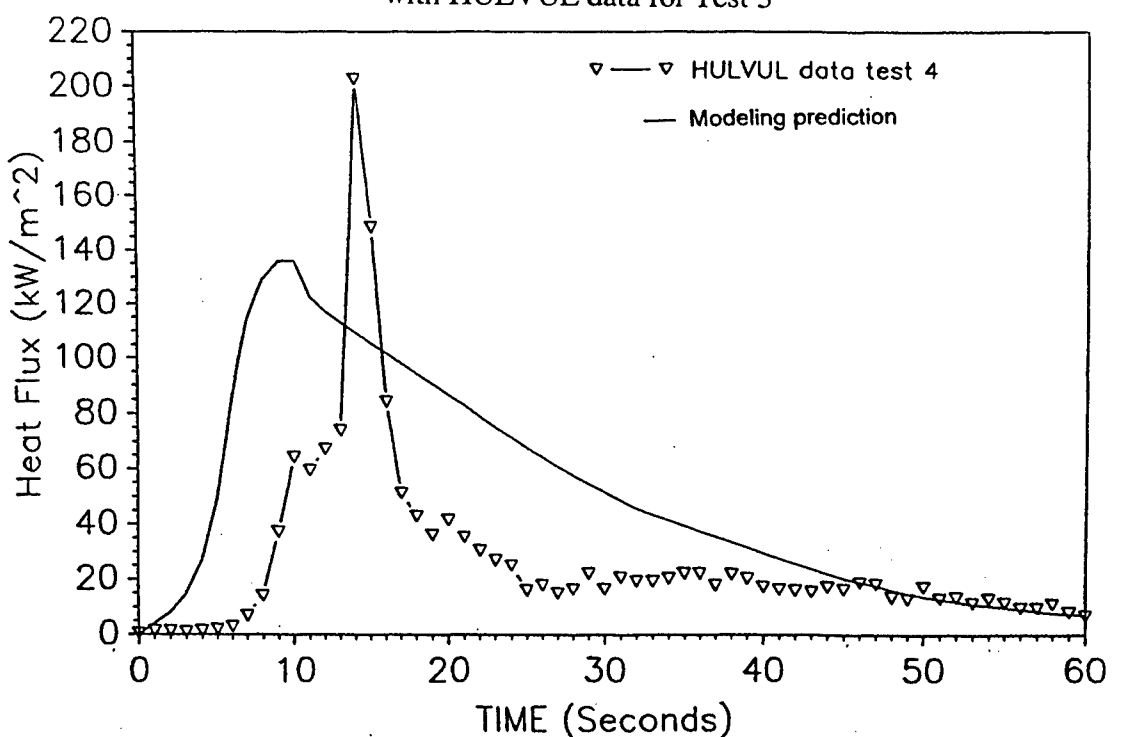

Figure A - 15. Modeling prediction of heat flux at floor level as compared with HULVUL data for Test 4

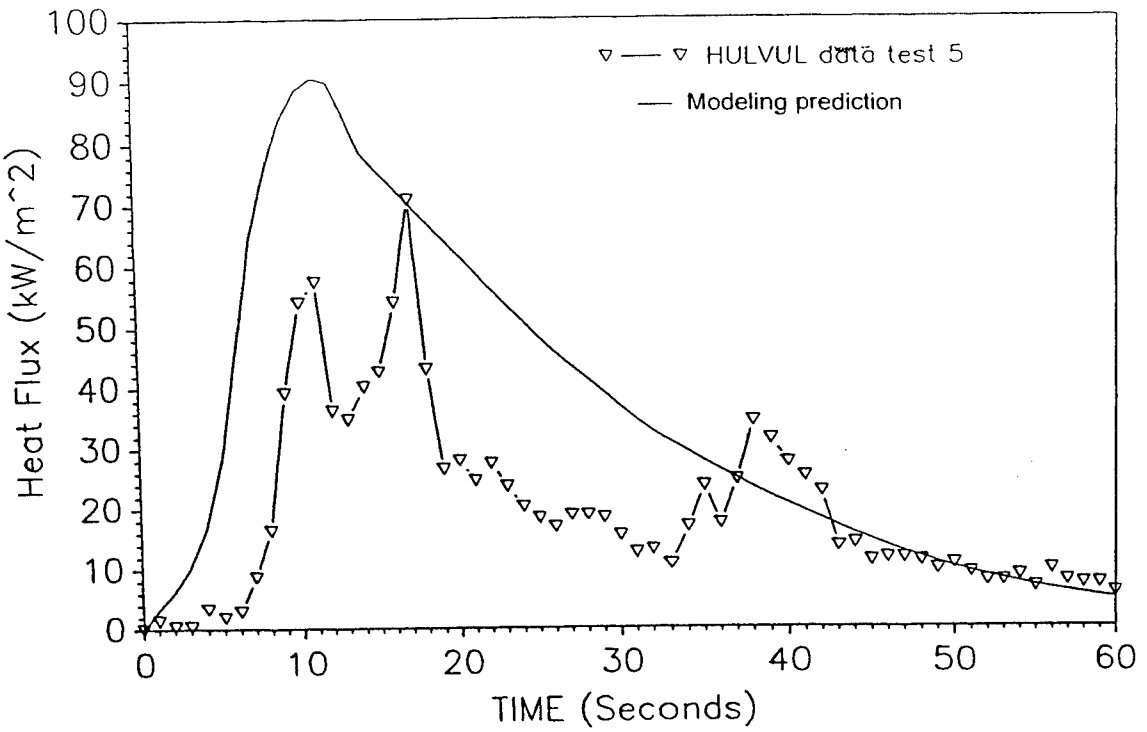

Figure A - 16. Modeling prediction of heat flux at floor level as compared with HULVUL data for Test 5

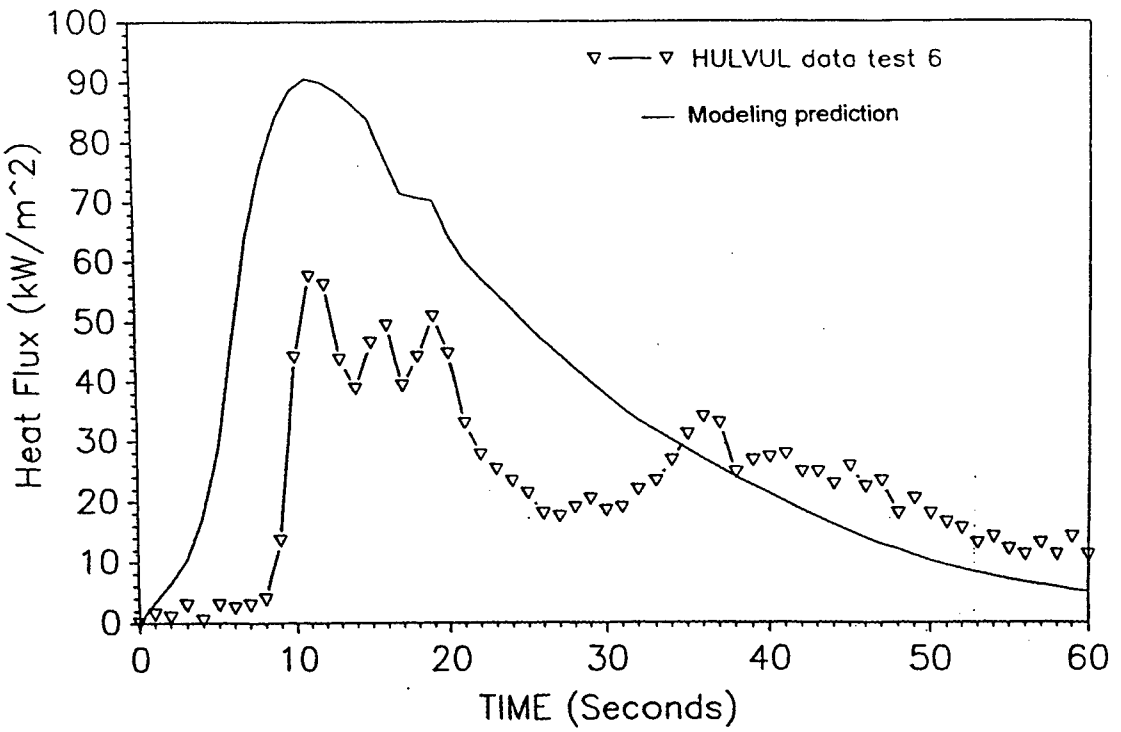

Figure A - 17. Modeling prediction of heat flux at floor level as compared with HULVUL data for Test 6

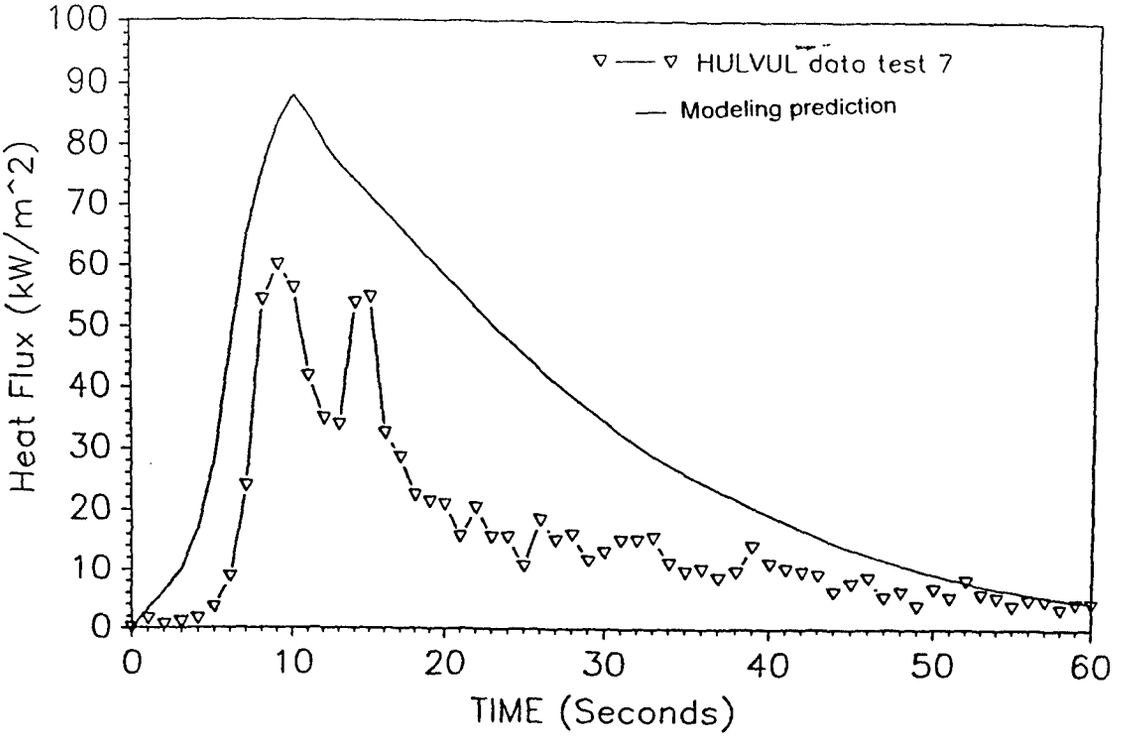

Figure A - 18. Modeling prediction of heat flux at floor level as compared with HULVUL data for Test 7

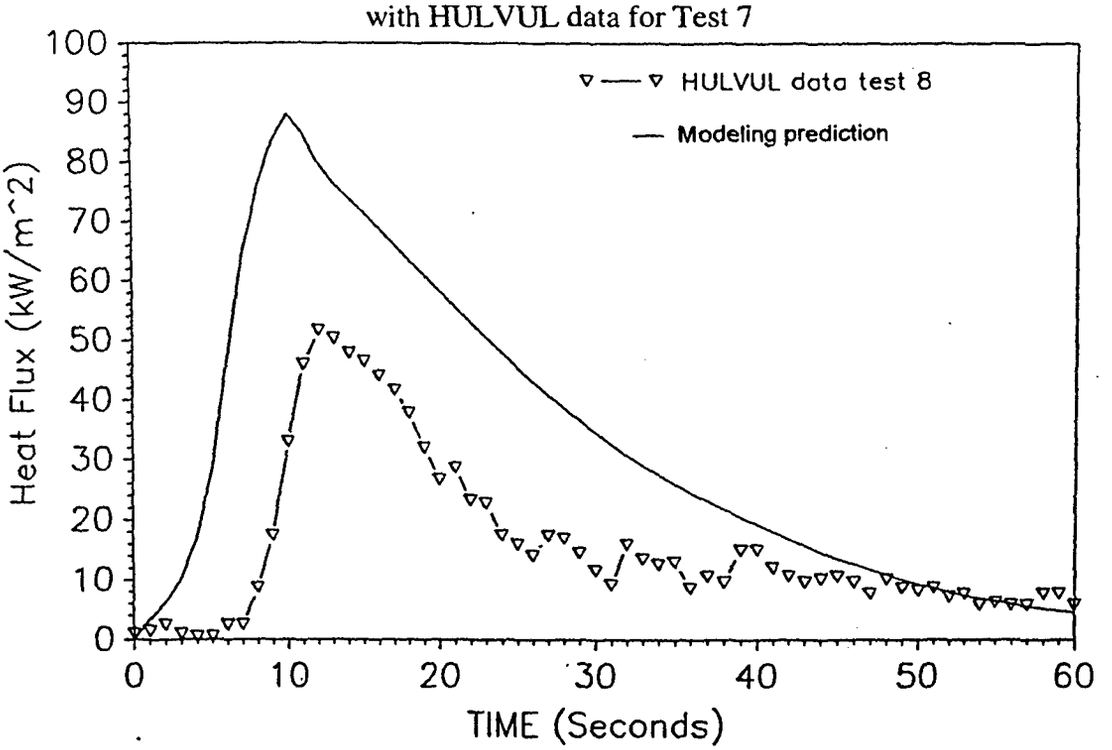

Figure A - 19. Modeling prediction of heat flux at floor level as compared with HULVUL data for Test 8

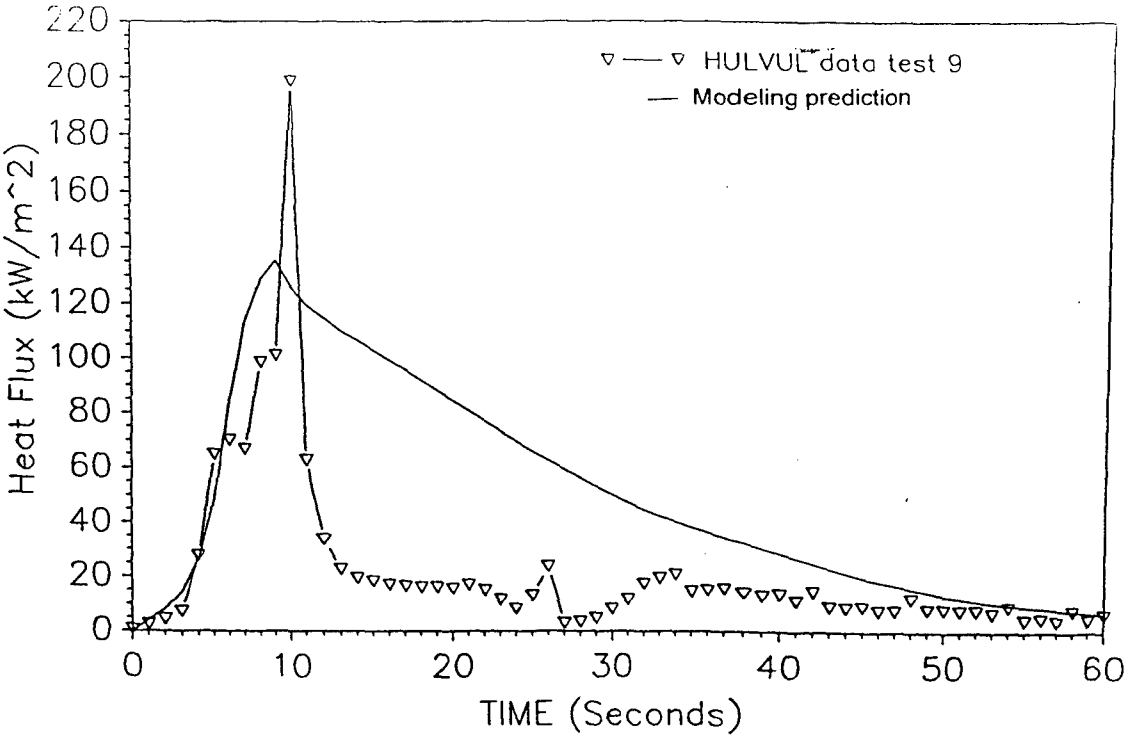

Figure A - 20. Modeling prediction of heat flux at floor level as compared with HULVUL data for Test 9

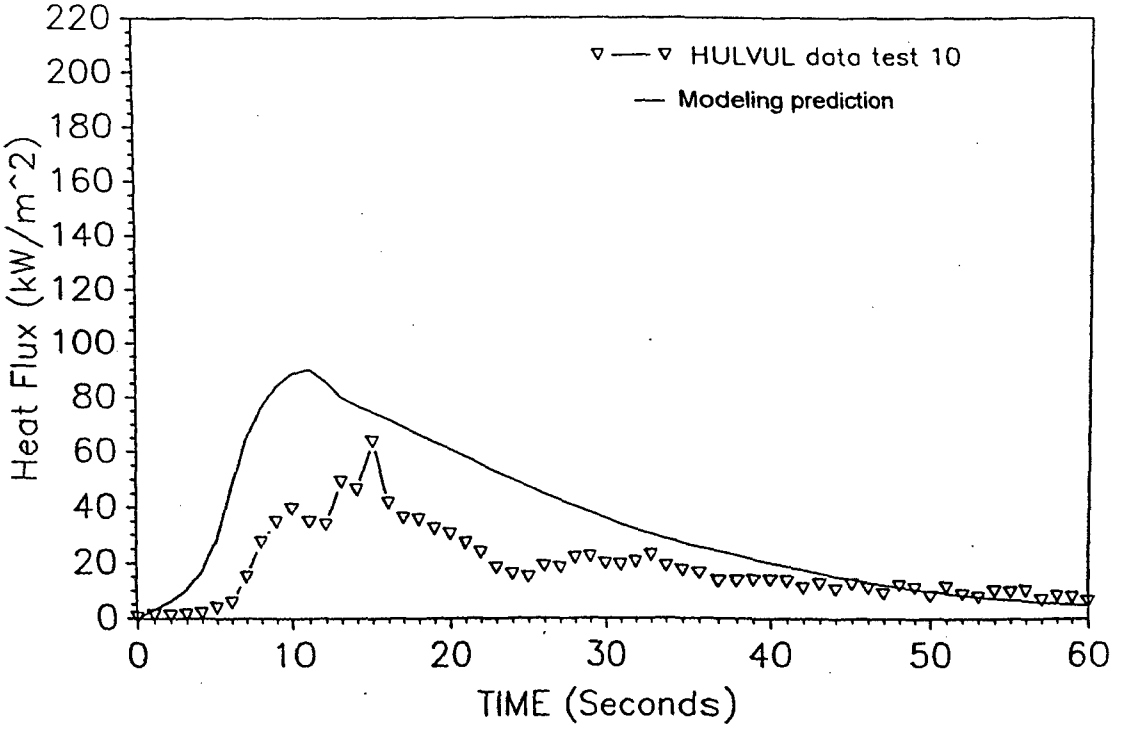

Figure A - 21. Hughes modeling prediction of heat flux at floor level as compared with HULVUL data for Test 10

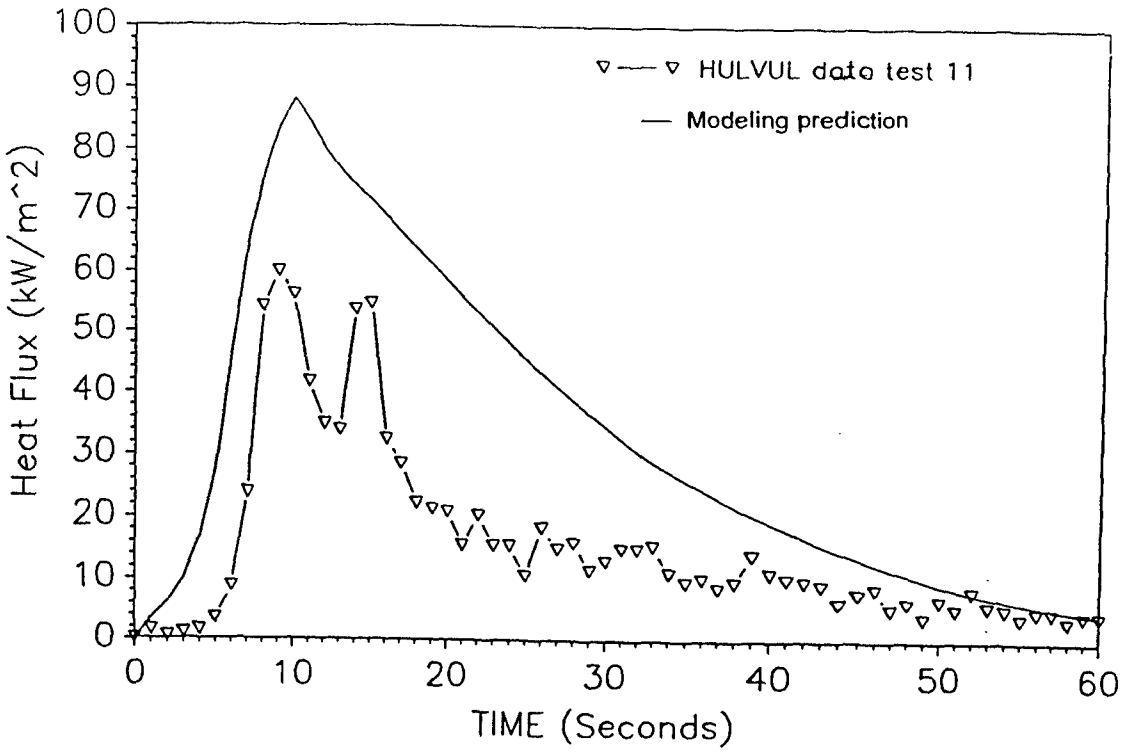

Figure A - 22. Modeling prediction of heat flux at floor level as compared with HULVUL data for Test 11

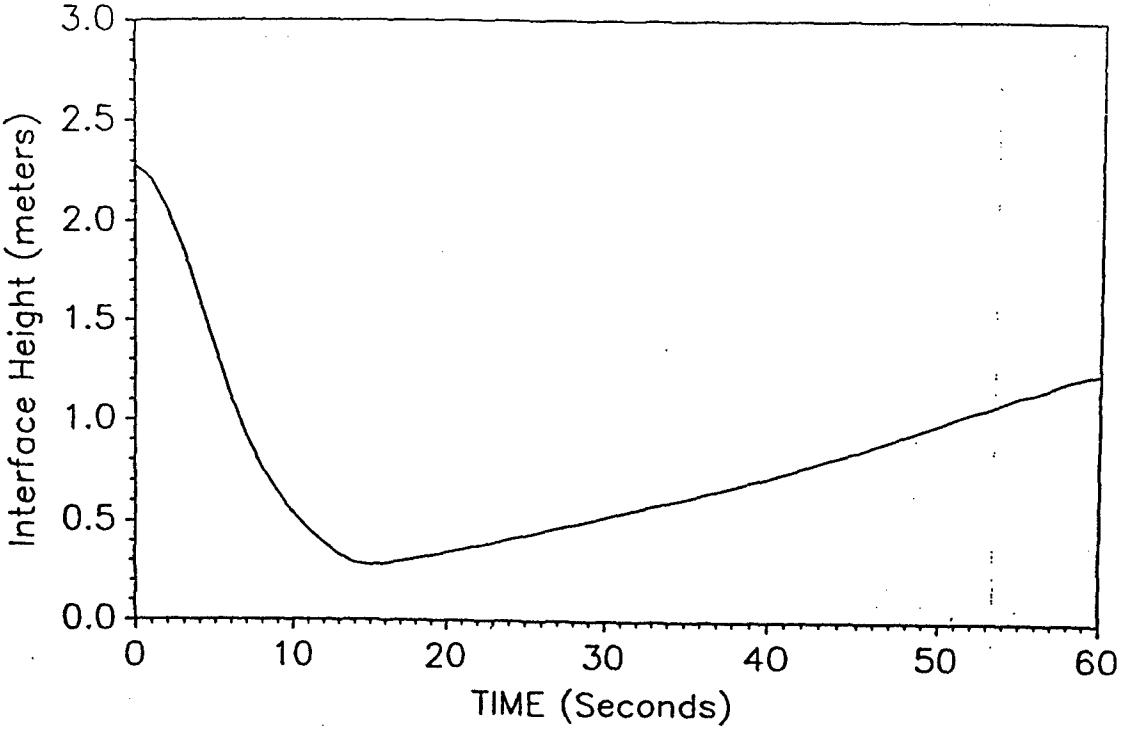

Figure A - 23. Modeling prediction of layer interface height for HULVUL Test 1

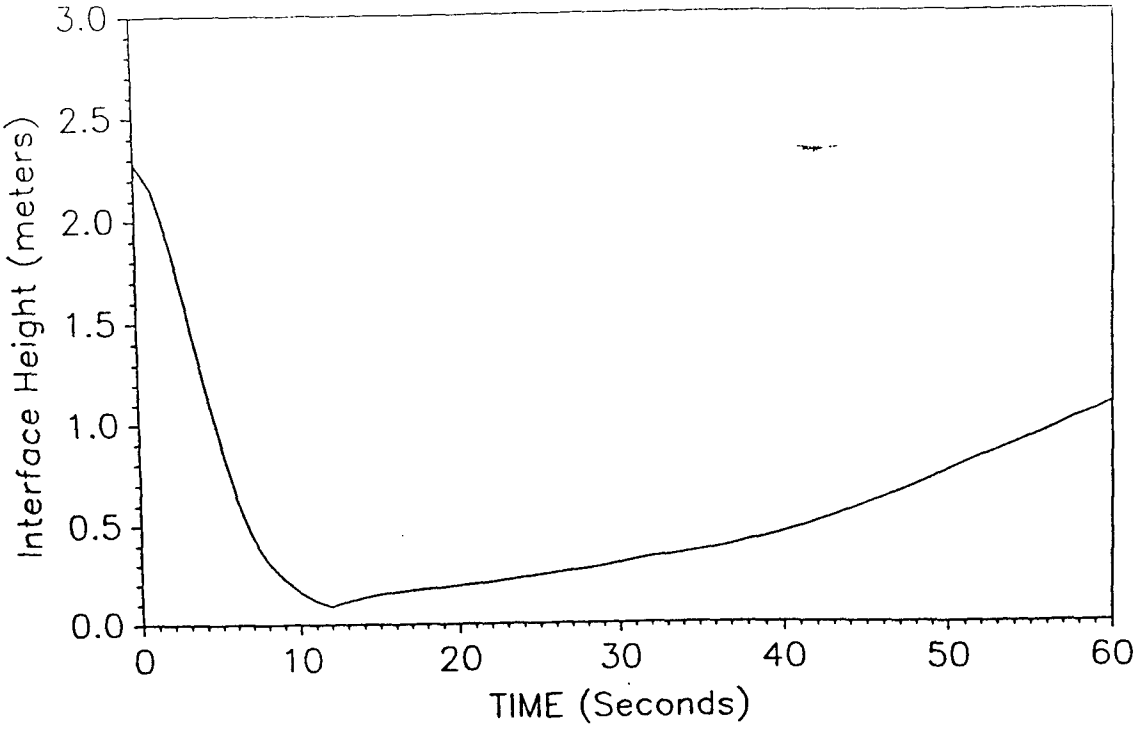

Figure A - 24. Hughes modeling prediction of layer interface height for HULVUL Test 2

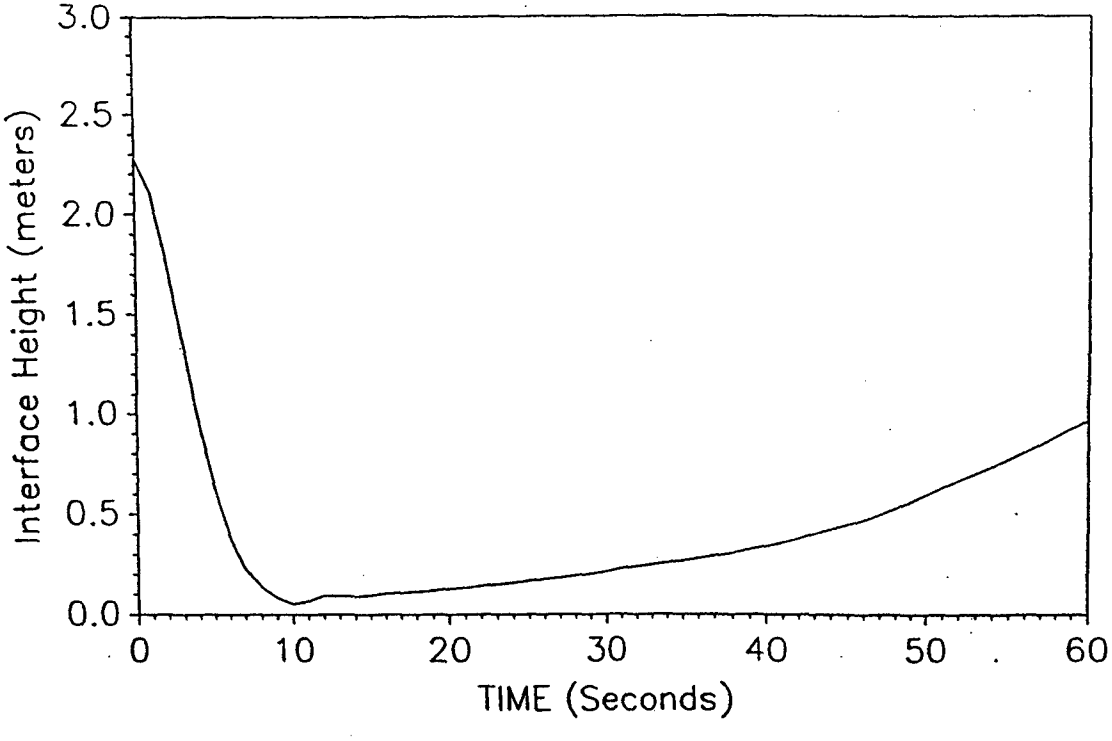

Figure A - 25. Modeling prediction of layer interface height for HULVUL Test 3

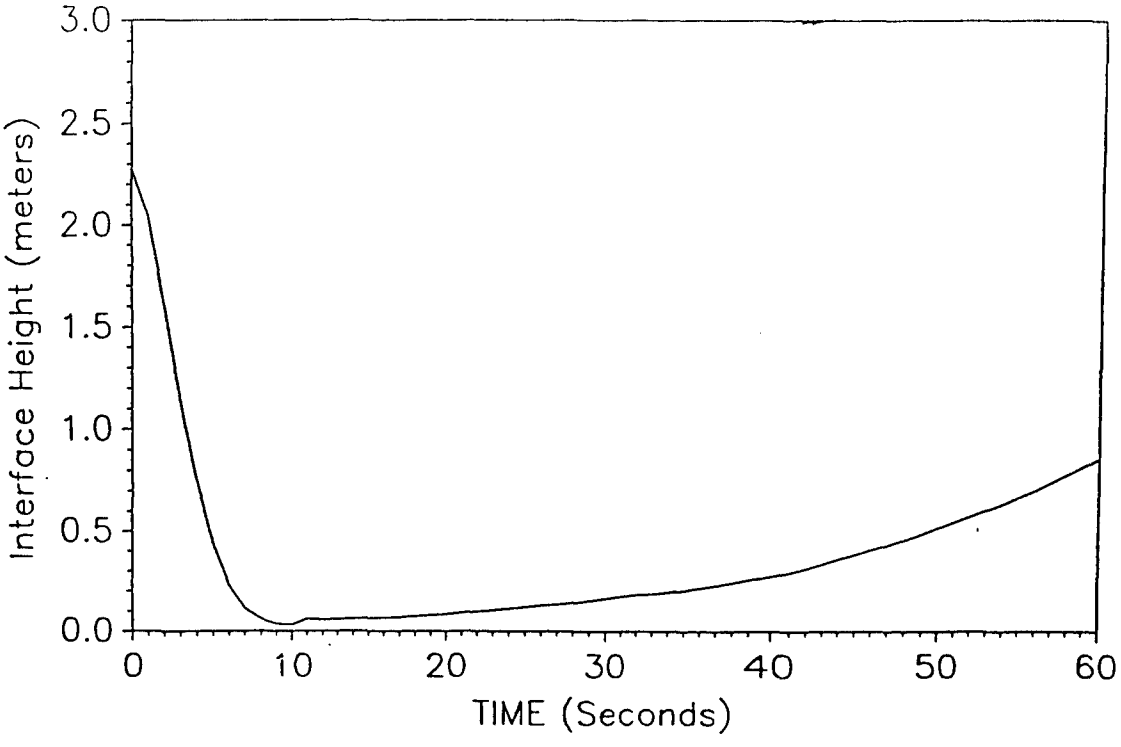

Figure A - 26. Modeling prediction of layer interface height for HULVUL Test 4

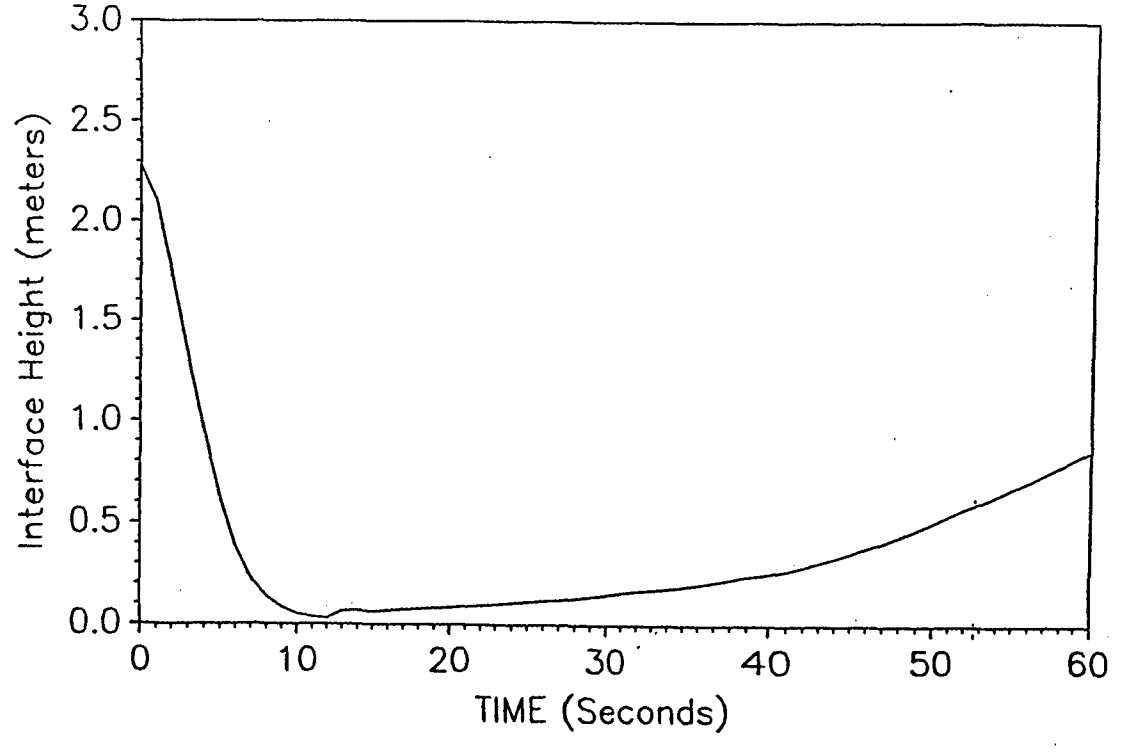

Figure A - 27. Modeling prediction of layer interface height for HULVUL Test 5

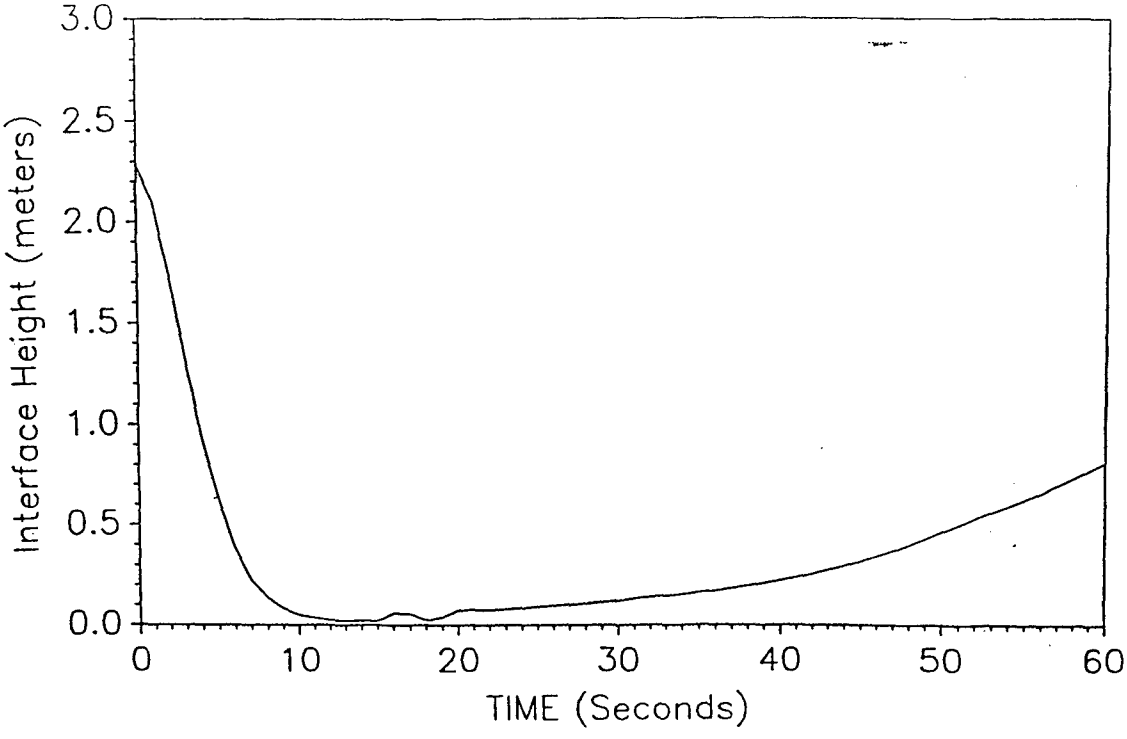

Figure A - 28. Modeling prediction of layer interface height for HULVUL Test 6

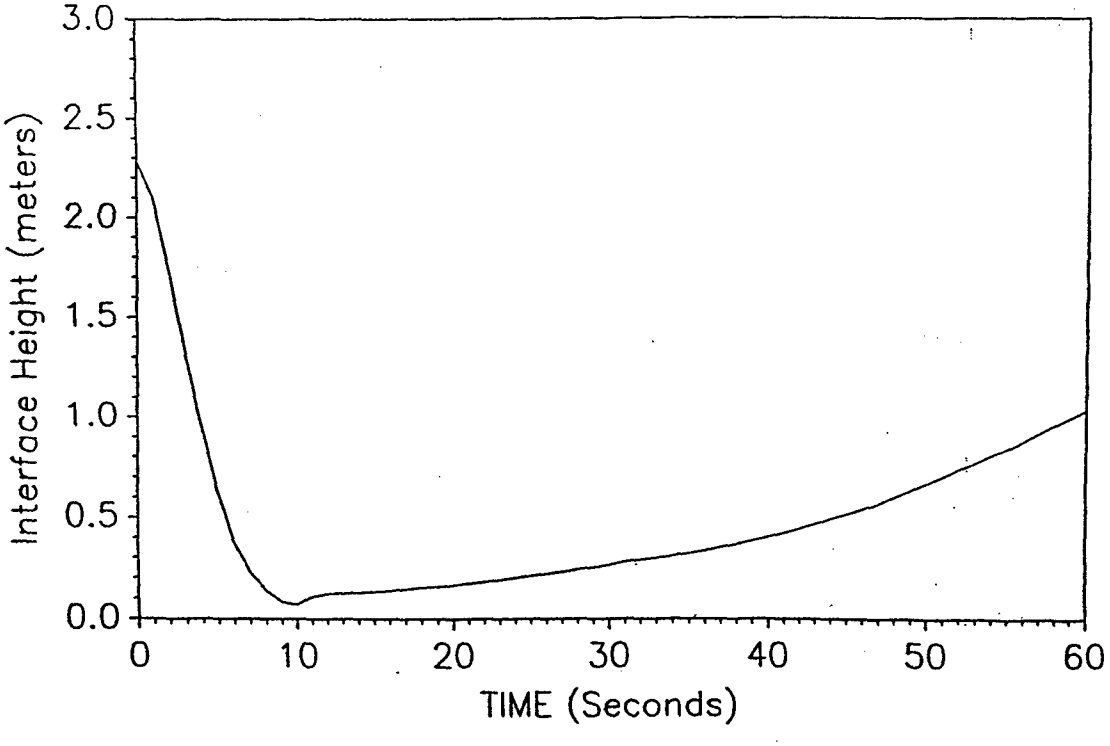

Figure A - 29. Modeling prediction of layer interface height for HULVUL Tests 7, 8, and 11

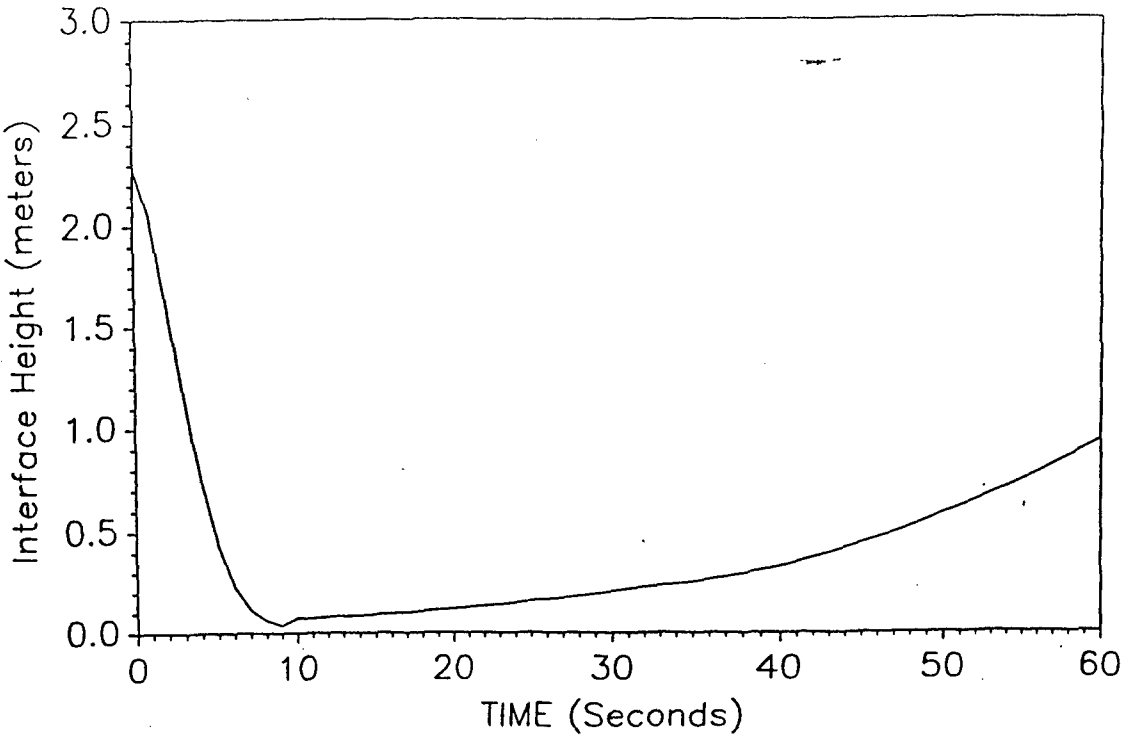

Figure A - 30. Modeling prediction of layer interface height for HULVUL Tests 9 and 11

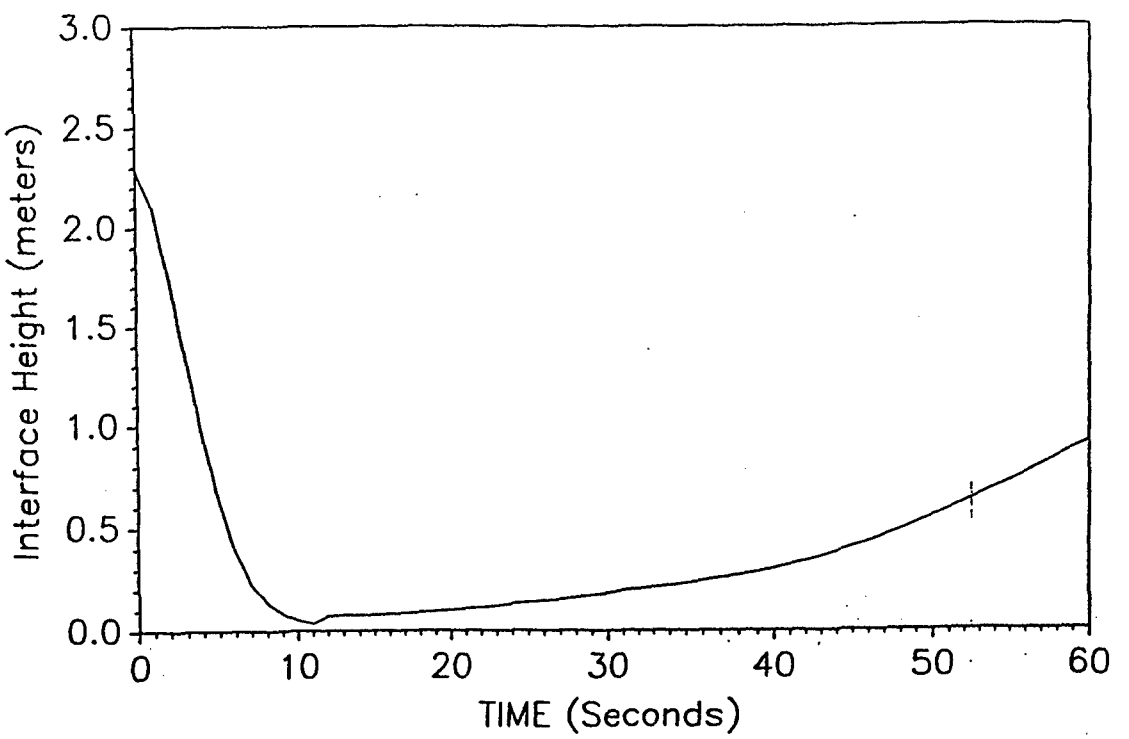

Figure A - 31. Modeling prediction of layer interface height for HULVUL Test 10